Loss of LRRC33-Dependent TGFβ1 Activation Enhances Antitumor Immunity and Checkpoint Blockade Therapy

Aiping Jiang[1,2], Yan Qin[1,2], and Timothy A. Springer[1,2]

ABSTRACT

TGFβ has multiple roles and gene products (TGFβ1, -β2, and -β3), which make global targeting of TGFβ undesirable. Expression of TGFβ requires association with milieu molecules, which localize TGFβ to the surface of specific cells or extracellular matrices. Here, we found that LRRC33 was specifically associated with TGFβ1, not TGFβ2 and TGFβ3, and was required for surface display and activation of TGFβ1 on tumor-infiltrating myeloid cells. Loss of LRRC33-dependent TGFβ1 activation slowed tumor growth and metastasis by enhancing innate and adaptive antitumor immunity in multiple mouse syngeneic tumor models. LRRC33 loss resulted in a more immunogenic microenvironment, with decreased myeloid-derived suppressor cells, more active $CD8^+$ T and NK cells, and more skewing toward tumor-suppressive M1 macrophages. LRRC33 loss and PD-1 blockade synergized in controlling B16.F10 tumor growth. Our results demonstrate the importance of LRRC33 in tumor biology and highlight the therapeutic potential of dual blockade of the LRRC33/TGFβ1 axis and PD-1/PD-L1 in cancer immunotherapy.

Introduction

The three TGFβs have many important biological roles, and TGFβ1 is especially important in regulating wound-healing, immune responses, and tumor biology. Mice deficient in TGFβ1 die within a few weeks after birth from uncontrolled lymphocyte proliferation and autoimmunity. TGFβ inhibits $CD8^+$ killer T cells and $CD4^+$ Th1 and Th2 cells but stimulates regulatory T cells (Tregs). TGFβ also inhibits killing by natural killer (NK) and NKT cells and inhibits migration and expression of coreceptors and cytokine effectors by dendritic cells (DC). Thus, TGFβ polarizes immune-infiltrating cells in tumor microenvironments (TME) towards nonresponsiveness (1, 2).

TGFβ expression correlates with poor prognosis for patients with cancer and has long been considered an important therapeutic target (3). TGFβ has emerged as an important tumor driver associated with anti-PD-1/PD-L1 resistance in metastatic melanoma (4), and inhibition of TGFβ enhances immune-checkpoint blockade efficacy in multiple preclinical tumor models (5–7). Myeloid cells in the TME play an important role in tumor progression (8–11). High infiltration of immune-suppressive myeloid cells correlates with poor prognosis and resistance to checkpoint blockade therapy. These cells include $Mac\text{-}1^+F4/80^+$ tumor-associated macrophages (TAM), $Gr\text{-}1^+Mac\text{-}1^+$ myeloid-derived suppressor cells (MDSC), and $Mac\text{-}1^+CD11c^+$ DCs, which infiltrate the TME in tumor-bearing mice, as well as in patients with cancer. Tumor-associated myeloid cells are the predominant sources of TGFβ1 in the TME (2) and are important in tumor immune-evasion (12). Hematopoietic cells preferentially express TGFβ1, and selective TGFβ1 inhibition is sufficient to overcome resistance to checkpoint blockade therapy (5, 13–15).

Here, we tested whether TGFβ1 associated with a specific milieu molecule, leucine-rich repeat-containing glycoprotein 33 (LRRC33; ref. 16), was important in tumor biology. Early in intracellular biosynthesis, the large, N-terminal pro-domain of TGFβ coassociates noncovalently and through disulfide bonds with milieu molecules. Besides LRRC33, milieu molecules include GARP (LRRC32) and latent TGFβ binding proteins (LTBP) 1, 3, and 4 (17). Before secretion of milieu molecule–TGFβ complexes, furin cleaves between the TGFβ pro- and growth factor domains. Milieu molecule–TGFβ complexes remain latent in the environment, where the milieu molecule anchors them on the cell surface or in the extracellular matrix until activation releases the growth factor from the complex. TGFβ1 is activated by integrins αVβ6 and αVβ8, which bind to an RGDLXXI/L motif in their prodomains and release the TGFβ growth factor from latency (17, 18). LRRC33 is 34% identical in amino acid sequence with its paralogue GARP, and both have transmembrane domains that localize them to cell surfaces. LRRC33 is expressed on myeloid cells, especially on monocytic cells including microglia and macrophages, that also express TGFβ1, and hence make LRRC33–TGFβ1 complexes. This complex appears to be the only type of TGFβ1 complex in macrophages and microglia, as demonstrated in *Lrrc33*$^{-/-}$ mice, where these myeloid cells are deficient not only in surface expression of LRRC33, but also in cell surface expression and activation of TGFβ1 (16).

In this study, we prefer to use the original gene name *Lrrc33*, which is functionally agnostic. Several different functions have been ascribed to this gene, including acting as a milieu molecule for TGFβ1 (16), negatively regulating Toll-like receptors (19), and acting as a negative regulator of reactive oxygen species (*NRROS*; ref. 20). This gene was renamed from *LRRC33* after a request to the Human Genome Organization (HUGO) Gene Nomenclature Committee. The name for the protein remains LRRC33, and UniProt changed its longer name to "TGFβ activator LRRC33" after the demonstration that LRRC33 is a milieu molecule required for expression and activation of TGFβ1 (16). The characterization of LRRC33 as a negative regulator of reactive oxygen species has been questioned (16). In brief, the effects on macrophage reactive oxygen species (20) and innate immune function in *Lrrc33*$^{-/-}$ mice (19) are readily explained by the findings that TGFβ is a potent negative regulator of reactive oxygen species generation by

[1]Program in Cellular and Molecular Medicine, Boston Children's Hospital, Boston, Massachusetts. [2]Department of Biological Chemistry and Molecular Pharmacology, Harvard Medical School, Boston, Massachusetts.

Note: Supplementary data for this article are available at Cancer Immunology Research Online (http://cancerimmunolres.aacrjournals.org/).

Current address for Y. Qin: Fuhong Therapeutics, Lexington, Massachusetts.

Corresponding Author: Timothy A. Springer, PCMM/BCMP, Boston Children's Hospital/Harvard Medical School, 3 Blackfan Circle, Boston, MA 02118. E-mail: springer@crystal.harvard.edu

Cancer Immunol Res 2022;10:453–67

doi: 10.1158/2326-6066.CIR-21-0593

macrophages (21) and suppresses innate immune function (1), respectively. The striking phenotype of ascending paraparesis and death by five months in *Lrrc33*$^{-/-}$ mice was not revealed in the original report (20); however, a subsequent report by the same group shows that mice deficient in both *Lrrc*33 and *Cybb*, an essential component of oxidases, have the same neurologic defects as *Lrrc33*-deficient mice (22). Thus, reactive oxygen species are unrelated to the only overt phenotype of *Lrrc33*-deficient mice. In contrast, the phenotype of *Lrrc33*-deficient mice is similar to TGFβ1-deficient mice carrying a TGFβ1 transgene in T lymphocytes to protect against autoimmunity (23) and to mice deficient in the TGFβ1-activating integrin αVβ8 (24, 25). Patients deficient in *LRRC33* (reported as *NRROS* following requirements of human genetics journals to use the HUGO gene name) are reported to have severe infantile-onset neurodegeneration, with similarities to human loss of TGFβ1 function and to the phenotype of *Lrrc33* deficiency in mice (26, 27). Our previous findings that LRRC33 associates with TGFβ1 were independently confirmed. Complexes with wild-type LRRC33 and TGFβ1 are expressed on the cell surface, whereas LRRC33 with C-terminal missense mutations can complex intracellularly with TGFβ1 and cannot be expressed on the cell surface (26). The authors of the reports on human deficiency have joined in requesting that HUGO change the gene name back to *LRRC33*.

Here, we found that LRRC33 associates with TGFβ1 and not TGFβ2 or TGFβ3. Genetic ablation of *Lrrc33* significantly decreased tumor growth and metastasis in several syngeneic tumor models and enhanced anti-PD-1 treatment efficacy. We also defined the cellular mechanisms underlying the role of LRRC33/TGFβ1 complexes in downregulating immunity in the TME. Our studies reveal a more selective, cell type–specific cancer target for blocking TGFβ1 in the TME.

Materials and Methods

Study approval and mice

All animal experiments were approved by the Institutional Animal Care and Use Committees (IACUC) at Harvard Medical School and Boston Children's Hospital. All *Lrrc33*$^{+/+}$ (WT), *Lrrc33*$^{+/-}$ (heterozygous), and *Lrrc33*$^{-/-}$ (KO) mice were on the C57BL6/NJ (CD45.2^{+}) background, had been further backcrossed onto C57BL6/NJ, and were genotyped and maintained as described (16). Mice with no noticeable neurologic symptoms (6–8 weeks old) were used for all experiments. All KO, heterozygous, and WT mice were littermates. B6 CD45.1 (Strain #002014) and C57BL/6J *Rag1*$^{-/-}$ mice (Strain #002216) were from The Jackson laboratory. *Lrrc33*$^{+/-}$ mice were bred with *Rag1*$^{-/-}$ mice to obtain F1 mice, among which *Lrrc33* heterozygote-genotyped mice were used for breeding. *Lrrc33*$^{-/-}$ offspring which lacked CD3^{+} T cells in tail vein blood, as shown by flow cytometry, were *Rag1*$^{-/-}$ and were used as *Lrrc33*$^{-/-}$ *Rag1*$^{-/-}$ mice; *Rag1*$^{-/-}$ mice used in experiments were littermates that were *Lrrc33*$^{+/+}$ and lacked CD3^{+} T cells.

Cell lines and culture

B16.F10 cells and LLC1 cells were purchased from the ATCC in 2017. MC38 cells and CAGA cells (28) were gifts from the Arlene Sharpe lab at Harvard Medical School and Thomas Thompson lab at University of Cincinnati, respectively. All cell lines were frozen in liquid nitrogen. For experiments, cell aliquots were thawed, and used for no more than 2 to 3 weeks, or about 5 to 10 passages. B16.F10 cells produced black tumors and metastases and were resistant to PD-1 antibody *in vivo* as reported, whereas MC38 cells were susceptible to PD-1 antibody *in vivo* as reported. CAGA cells produced luminescence after TGFβ stimulation as expected. Cells were cultured in DMEM supplemented with 10% FBS (Sigma-Aldrich), 4 mmol/L L-glutamine (Corning), and either 1% penicillin/streptomycin (Corning) or for CAGA cells 100 μg/mL of G418 (KSE Scientific). Expi293F cells were cultured in suspension in Expi293 Expression Medium (Life Technologies) with no antibiotics. Full-length αV-GFP, β6, Flag-tagged proTGFβ1, proTGFβ2, proTGFβ3, and HA-tagged LRRC33 or GARP were transiently transfected into Expi293F cells using jetPRIME (Polyplus) according to the manufacturer's instructions. Flow cytometry was used to detect αVβ6 expression via GFP and tagged proteins by staining with anti-DYKDDDDK Flag (clone L5) and anti-HA (clone 12CA5). All cells were cultured at 37°C in a humidified 5% CO_2 atmosphere. All cell lines were tested every 3 months and found free from mycoplasma contamination. Transiently transfected cells were used immediately 48 hours after.

Immune cell subsets in naïve WT and *Irrc33*$^{-/-}$ mice

Spleen, thymus, and lung tissues were taken from 7-week-old WT and *Lrrc33*$^{-/-}$ mice. The flat end of the syringe plunger was used to mince the spleen or thymus in a 70-μm cell strainer by crushing the tissues in gentle circular motions to release the splenocytes or thymocytes. For lung extravascular DC analysis, mice were injected intravenously with 3 μg of mouse CD45.2 antibody to label intravascular leukocytes, and mice were euthanized 3 minutes postinjection. Lungs were harvested and digested in 1 mg/mL of Liberase TM (Roche) and 20 μg/mL of DNaseI (Roche) for 20 minutes at 37°C; ammonium–chloride–potassium (ACK) lysing buffer (Thermo Fisher Scientific) was used to lyse red blood cells.

Mouse syngeneic tumor models and pulmonary metastasis

Tumor cells (1×10^5 B16.F10, 3×10^5 MC38, or 1×10^4 LLC1 cells) in 100 μL PBS were subcutaneously injected into the shaved right flank of mice (C57BL6/NJ *Lrrc33*$^{+/+}$, *Lrrc33*$^{+/-}$, *Lrrc33*$^{-/-}$, *Rag1*$^{-/-}$, and *Lrrc33*$^{-/-}$*Rag1*$^{-/-}$). Once palpable, tumors were measured every 2 to 3 days (long diameter and short diameter) with a caliper. KO mice were housed in the same cages as control WT or heterozygote mice, which supported better survival of KO mice and also facilitated blinded tumor size measurements (randomly picking up each mouse and reading/recording its tumor size and animal ID number without knowing its genotype). WT recipient mice that received WT or KO bone marrow were housed in separate cages and therefore were not studied blinded. Tumor volume was determined using the formula for a solid ellipsoid: $L \times W^2/2$, where L is the longer diameter and W is the shorter diameter. Mice were sacrificed when tumors were ulcerated, bleeding, or >2 cm. For antibody treatments, mice were given 10 mg/kg antibody via intraperitoneal injection every 3 days, starting when tumors became palpable, with an average tumor volume of 30 mm^3. Dosing schedule is shown in figures. The following antibodies were used: anti-PD-1 (BioXCell clone RMP1–14; catalog no. BE0146), 21D1 (a gift from Scholar Rock, Inc.; ref. 29), IgG control (BioXCell Rat IgG2a), or human IgG4 (recombinant IgG expressed in Expi293F cells and purified from supernatant by protein G and Sephadex S200 chromatography). For treatment with PD-1 or 21D1 antibodies, we chose mice with similar tumor sizes for antibody and isotype control treatments. A larger number of WT and KO mice were injected with tumors than needed for treatment studies. On the first day of treatment, tumors were measured and ranked by size. A sufficient number of mouse pairs with tumors of similar size were chosen and one from each pair was randomly assigned to the treatment group and the other in the pair to the isotype control group.

For assessment of pulmonary metastasis, 3×10^5 B16.F10 cells were transferred intravenously via tail-vein injection. After 14 days, lungs were perfused using PBS and fixed overnight in 4% paraformaldehyde (PFA) solution. Fixed tissues were sent to the Rodent Pathology Core at Harvard Medical School for paraffin embedding, sectioning, and hematoxylin and eosin histologic staining. The number of metastatic foci was determined using an Olympus BX51 microscope on sections taken every 100 μm throughout the whole lung for at least 5 animals per group.

Whole bone marrow transplantation

Congenic mouse transplant recipients (10-week-old CD45.1$^+$ C57BL6/NJ) were lethally irradiated (950 rad; RS-2000, Rad Source) and tail-vein injected with 8×10^6 freshly harvested whole bone marrow cells from femurs of WT or *Lrrc33*$^{-/-}$ donor mice (10-week-old CD45.2$^+$ C57BL6/NJ). Transplant recipients were given water containing 30 mg/L neomycin sulfate, 30 mg/L kanamycin sulfate and 50 mg/L gentamycin sulfate for 4 weeks. MC38 tumor cells were injected 10 weeks posttransplant when CD45.2$^+$ bone marrow chimerism averaged over 90% in peripheral blood, showing successful transplantation.

Cell isolation

B16F10 or MC38 tumors were excised and weighed 14 days after subcutaneous tumor cell injection, cut into 2-mm-sized pieces, and enzymatically dissociated in RPMI1640 medium with 5% FBS, 0.1% 2-mercaptoethanol, 1 mg/mL collagenase IV (Roche), 20 μg/mL Dnase I (Roche) at 37°C for 30 minutes during rotation at 180 rpm. Cell mixtures were pipetted up and down to further dissociate cells and then filtered through a 70-μm cell strainer to obtain single-cell suspensions. To isolate tumor-infiltrating leukocytes, cells were centrifuged, and pellets were resuspended in 40% Percoll (GE Healthcare) and slowly layered on 70% Percoll for centrifugation at 2,200 rpm for 30 minutes at room temperature. Leukocytes from the 40% to 70% Percoll interface and other cells from the pellet were washed twice with PBS.

For myeloid cell purification, Petri dishes (100 mm × 15 mm, Falcon REF351029, not tissue culture-treated) were precoated with 5 μg/mL of specific antibodies in 0.05 M pH 9.0 Tris buffer at 4°C overnight and then washed with PBS before adding 1×10^7 cells in RPMI1640 medium with 10% FBS. After attachment at 37°C for 2 hours in a 5% CO_2 incubator, dishes were washed four times with PBS, adherent cells were detached with 0.25% trypsin/0. 5 mmol/L EDTA (Corning) in PBS, diluted in RPMI1640/10% FBS, and centrifuged. Cells were either resuspended in RPMI1640/10% FBS for further purification, in FreeStyle medium for TGFβ assays, or in TRizol (Invitrogen) for RNA isolation.

Using the above protocol, whole bone marrow cells or tumor leukocytes were panned with anti-CD3 (clone 17A2, Biolegend) and anti-CD19 (clone 6D5, Biolegend) to obtain T and B cells for RNA isolation. Nonadherent cells were then added to anti-Mac-1-coated (clone M1/70, Biolegend) plates to enrich myeloid cells for RNA isolation or for further purification. To further purify myeloid populations, cells were resuspended as above and added to dishes precoated with antibodies against F4/80 (clone BM8, Biolegend), CD11c (clone N418, Biolegend), and Gr-1 (clone RB6–8C5, Biolegend) to enrich macrophages, DCs, and MDSCs or granulocytes, respectively.

Flow cytometry

Flow cytometry on tumor samples from models was not performed in a blinded manner. For cell surface staining, cells were preincubated with 5 μg/mL of anti-mouse CD16/32 Fc blocker (Biolegend, catalog no. 101319) in FACS buffer (2% FBS/PBS) for 15 minutes on ice and stained with 2 μg/mL of fluorophore-conjugated antibodies at 4°C for another 30 minutes. Antibodies to surface markers were all from Biolegend: Alexa Fluor-647 anti-mouse CD45.2 (clone 104), Pacific Blue anti-mouse CD45 (clone 30-F11), Alexa Fluor-700 anti-mouse CD45.2 (clone 104), FITC-anti-mouse CD3 (clone 17A2), PE-anti-mouse CD4 (clone GK1.5), PE-anti-mouse CD8a (clone 53–6.7), APC-anti-mouse CD8a (clone 53–6.7), APC-anti-mouse NK1.1 (clone pk136), PE-Cy7- anti-mouse Mac-1 (clone M1/70), PE-anti-mouse F4/80 (clone BM8), PE-anti-mouse Gr1 (clone RB6–8C5), APC-anti-mouse Ly-6C (clone HK1.4), FITC-anti-mouse Ly6G (clone 1A8), Brilliant Violet 421 anti-mouse CD103 (clone 2E7), APC anti-mouse CD103 (clone 2E7), PE-anti-mouse CD11c (clone HL3), APC-anti-mouse MHC-II (clone AF6–120.1), FITC anti-mouse MHC-II (clone AF6–120.1), PE-anti-mouse CD326 (EpCAM; clone caa7–9G8), anti-alpha smooth muscle actin (α-SMA, clone 1A4), and Brilliant Violet 421 anti-mouse TGF-β1 prodomain (clone TW7–16B4; ref. 30).

For intracellular staining, cells were first treated and stained for cell surface markers as described above, and then fixed and permeabilized with the BD Cytofix/Cytoperm Kit and stained according to the manufacturer's instructions. For intracellular TNFα and IFNγ, prior to cell surface staining, cells were cultured in RPMI1640 medium supplemented with 10% FBS and BD leukocyte activation cocktail following manufacturer's instruction at 37°C for 4 hours. To detect Foxp3, the eBioscience Foxp3/Transcription Factor Staining Buffer Set was used following the manufacturer's instructions. Antibodies were from Biolegend: PE anti-human/mouse granzyme B (clone QA18A28), APC anti-mouse TNFα (clone MP6-XT22), Brilliant Violet 421 rat anti-mouse IFNγ (clone XMG1.2), Brilliant Violet 421 anti-mouse Foxp3 (clone MF-14), and PE-anti-mouse CD206 (clone C068C2). For phosphorylated (p)SMAD staining, cells were fixed and permeabilized using BD Phosflow Lyse/Fix Buffer and BD Phosflow Perm Buffer III and stained with BD Phosflow Alexa Fluor-647 anti-Smad2 (pS465/pS467)/Smad3 (pS423/pS425; clone O72–670; BD Biosciences) following the manufacturer's instructions. Samples were run on a BD Canto II, and data analysis was performed using FlowJo.

TGFβ activation assay

CAGA cells (1.5×10^4/well) seeded in 96-well flat plates were cultured in DMEM supplemented with 10% FBS and 1% penicillin/streptomycin in a 5% CO_2 incubator at 37°C. After 4 hours, plates were inverted, flicked, and wicked to remove excess medium. Purified myeloid, B16.F10, or MC38 cells (1×10^5 unless otherwise indicated) were cocultured with mock or αVβ6 transiently transfected Expi293F cells (2×10^4) in a total of 100 μL Freestyle medium; in some cases, medium included 21D1 anti-TGFβ or human IgG4 isotype control. For standard curves, recombinant human TGFβ1 growth factor (#T7039, Sigma) at 20 ng/mL and 11 2-fold dilutions thereof in Freestyle medium was added to CAGA cells. After 24 hours, supernatants were removed, and 40 μL nondiluted cell lysate was assayed for luciferase activity using Luciferase Assay System (Promega, catalog no. E1501) according to the manufacturer's instructions. Plates were read on a Biotek Synergy H1. TGFβ concentrations were calculated in PRISM9 from the luciferase activity using a standard curve.

qRT-PCR

RNA from B16F10 and MC38 cell lines, CD45$^-$ and CD45$^+$ cells, lymphocytes, myeloid cells, and tumor cells isolated from tumors was

extracted using the Direct-zol RNA Mini Prep Kit (Zymo Research) and 1 μg of RNA was reverse-transcribed using SuperScript II (Life Technologies) with oligo(dT18) in 10 μL total volume according to the manufacturer's instruction. One microliter of 5 × diluted cDNA product was used for template in qRT-PCR, which was performed using the Power SYBR Green PCR Master Mix (Invitrogen) on a CFX-Connect detection system (Bio-Rad) with Bio-Rad CFX Manager 3.1 software. Duplicate wells were performed for each sample and mRNA expression was determined relative to *Gapdh* (ΔCt = Ct gene of interest − Ct *gapdh*) with Ct representing cycle threshold. Primers used to murine genes were as follows: *Lrrc33* forward ACTGCAGCTTCCCAAGGA, *Lrrc33* reverse TGGGTACCGAAGCAAGGT; *Tgfb1* forward CTCCCGTGGCTTCTAGTGC, *Tgfb1* reverse GCCTTAGTTTGGACAGGATCTG; *Tgfb2* forward CTTCGACGTGACAGACGCT, *Tgfb2* reverse GCAGGGGCAGTGTAAACTTATT; *Tgfb3* forward CCTGGCCCTGCTGAACTTG, *Tgfb3* reverse TTGATGTGGCCGAAGTCCAAC; *Gapdh* forward GTTGTCTCCTGCGACTTCA, *Gapdh* reverse GGTGGTCCAGGGTTTCTTA.

Flow cytometry of Expi293f transfectants

Flag-tagged TGFβs and HA-tagged LRRC33 or GARP were transfected into Expi293F cells as described above. After 48 hours, cells were incubated with the primary antibodies in FACS buffer (PBS with 1% BSA) on ice for 30 minutes at 2 μg/mL: APC anti-DYKDDDDK tag (clone L5, Biolegend) and mouse anti-HA which was purified by protein G and Sephadex S200 chromatograpy from supernatant of 12CA5 hybridoma (31). After washing, the cells were incubated with Alexa 647-goat anti-mouse IgG (H+L; Invitrogen) secondary antibody for 30 minutes, washed, and analyzed on a FACS Canto II (BD Biosciences) and analyzed with FlowJo.

Immunoprecipitation (IP) and Western blot (WB)

Flag-tagged TGFβs and HA-tagged LRRC33 or GARP-Expi293F transfectants (~1×10^7/ml) were lysed at 4°C for 30 minutes in 500 μL of 150 mmol/L NaCl, 50 mmol/L Tris-HCL pH 8.0, 1% Triton-x100 (Sigma-Aldrich), 0.1% SDS (Sigma-Aldrich), 0.5% sodium deoxycholate, 1 mmol/L EDTA, and protease inhibitor cocktail (Roche) and centrifuged at 14,000 rpm at 4°C for 5 minutes. For IP, cell lysates (~400 μL) were incubated with 2 μg/mL of anti-Flag M2 (Sigma, F1804) overnight at 4°C with rotation and then 10 μL of protein G Sepharose beads (50% suspension in PBS; GE Healthcare) was added for 2 hours at 4°C with rotation. For WBs, 12.5 μL of 5× SDS sample buffer was added to 50 μL of cell lysate or 60 μL of 1× SDS sample buffer was added to pelleted, washed beads from IP. Samples were heated at 95°C in sample buffer containing 5 mmol/L N-ethylmaleimide (Calbiochem) or 5% β-mercaptoethanol and 12 μL per lane was subjected to nonreducing and reducing SDS-PAGE, respectively. Proteins were transferred to PVDF membrane (Bio-Rad) using Trans-Blot Turbo System (Bio-Rad) and probed with 2 μg/mL of specific antibodies (anti-Flag M2, Sigma F1804; anti-HA, 12CA5), and detected with 1 μg/mL of HRP-conjugated secondary antibodies (Abcam, ab6789). Blots were developed using the SuperSignal West Pico Plus Chemiluminescent Substrate (Thermo Fisher Scientific) and were imaged using an iBright FL1000 imager (Invitrogen).

Statistical analyses

For flow cytometry data, statistical analyses were performed using GraphPad Prism 9 software, and statistical significance was determined by unpaired Student *t* test (*, $P < 0.05$; **, $P < 0.01$; ***, $P < 0.001$).

Results

TGFβ1 specifically associates with LRRC33

LRRC33 can form noncovalent complexes, as well as covalent complexes, through disulfide bonds with TGFβ1 (16), but complex formation with other TGFβs has not been tested. GARP is a paralog of LRRC33 with 34% sequence identity, associates with TGFβ1, and has a role in tumor immunity (32), but like LRRC33, whether it can associate with TGFβ2 and TGFβ3 is uncharacterized. To better understand the roles of both LRRC33 and GARP in modulating tumor immune responses, we examined their specificity for different TGFβ isoforms. Flag-tagged TGFβs and HA-tagged LRRC33 or GARP were expressed together or separately in Expi293F cells. Expression of TGFβ1 on the cell surface was increased by coexpression with either LRRC33 or GARP (**Fig. 1A**). In contrast, LRRC33 did not promote TGFβ2 or TGFβ3 expression on the cell surface, whereas GARP augmented TGFβ2 and TGFβ3 expression on the cell surface (**Fig. 1A**). Furthermore, LRRC33 expression on the cell surface was increased by co-expression with TGFβ1, but not by TGFβ2 or TGFβ3 (**Fig. 1A**).

We next tested the association of LRRC33 and TGFβs by IP and WB. TGFβ1, TGFβ2, TGFβ3, and LRRC33 were detected in Expi293F transfectant cell lysates when TGFβ and LRRC33 were expressed individually or together (**Fig. 1B**, top and middle). HA-tagged LRRC33 interacted with all three FLAG-tagged TGFβs under reducing conditions when TGFβs were IP with LRRC33 and blotted with anti-HA antibody (**Fig. 1B**, bottom), although surface expression of LRRC33 was augmented only by TGFβ1, and LRRC33 selectively augmented surface expression of TGFβ1 (**Fig. 1A**). We, therefore, used a more stringent test and examined ability of LRRC33 to form disulfide bonds with the TGFβs. Nonreducing SDS-PAGE showed that only TGFβ1 formed a disulfide-linked complex of about 250 kDa with LRRC33 (**Fig. 1C**). Thus, among the three TGFβs, only TGFβ1/LRRC33 complexes were capable of forming milieu-molecule/TGFβ disulfide bonds and being transported to the cell surface. Taken together, these results suggest that TGFβ1, and not TGFβ2 and -β3, form biologically relevant complexes with LRRC33, whereas all three TGFβs form complexes with GARP.

Decreased tumor growth and absence of myeloid cell TGFβ1 expression in *Irrc33*$^{-/-}$ mice

We tested three different syngeneic tumor lines for growth in *Lrrc33*$^{-/-}$ mice after subcutaneous injection into the flank (**Fig. 2**). B16.F10 melanoma tumors grew more aggressively in WT mice than in *Lrrc33*$^{-/-}$ mice. Tumor volume was significantly less ($P = 0.04$), and the mass of explanted tumors was 5-fold lower in *Lrrc33*$^{-/-}$ mice (**Fig. 2A** and **B**). MC38 colon carcinoma cells also grew significantly more slowly and had significantly smaller (2.3-fold) masses at explant in *Lrrc33*$^{-/-}$ mice (**Fig. 2C** and **D**). Growth of B16.F10 melanoma and MC38 carcinoma tumors in heterozygous *Lrrc33*$^{+/-}$ mice was intermediate between growth in WT and homozygous *Lrrc33*$^{-/-}$ mice at all time points, but was not significantly different than in WT mice (Supplementary Fig. S1). Lewis lung carcinoma (LLC1) tumor cells also grew significantly more slowly and had smaller final masses in *Lrrc33*$^{-/-}$ mice, although the magnitude of the differences was less (**Fig. 2E** and **F**). Thus, all three tested tumor models showed significantly reduced growth in *Lrrc33*$^{-/-}$ mice.

Given the importance of TGFβ signaling in myeloid cells for tumor metastasis (33), we also tested a B16.F10 melanoma lung metastasis model. Fourteen days after intravenous injection of tumor cells, *Lrrc33*$^{-/-}$ mice displayed 56% fewer pulmonary

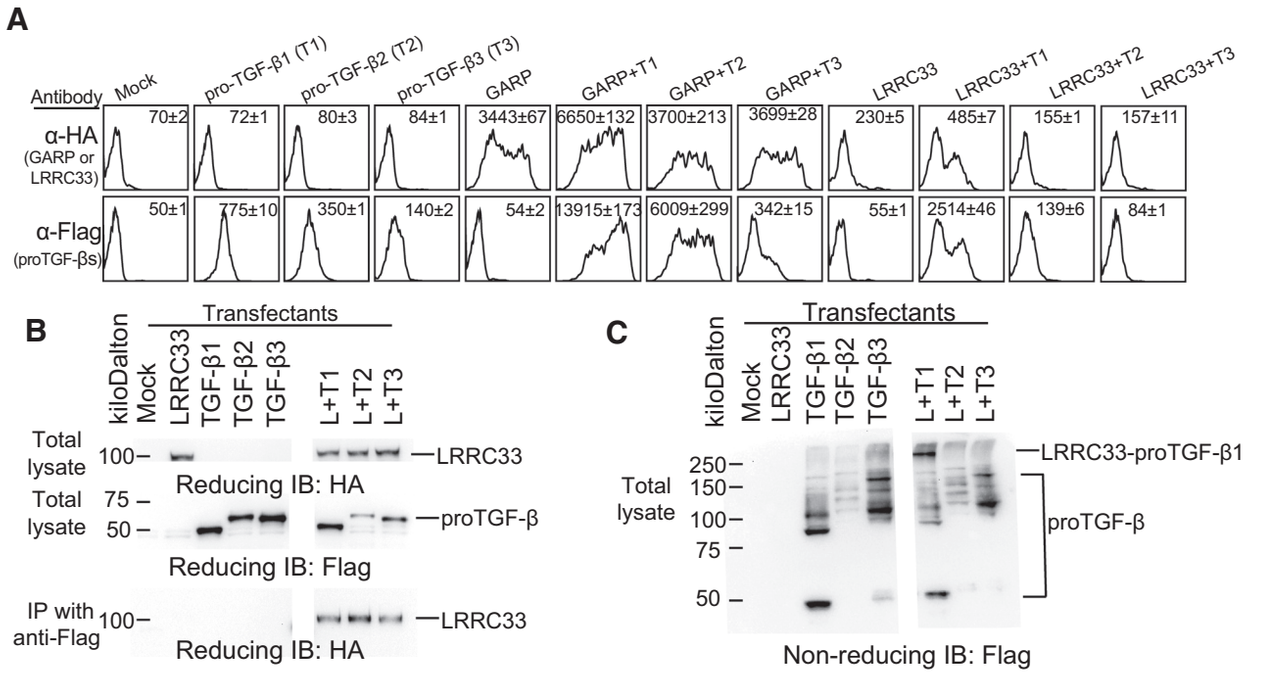

Figure 1.

LRRC33 is specific for TGFβ1. **A,** Expi293F cells were transfected with the indicated plasmids. 48 hours later, cell surface expression of HA-tagged LRRC33 or GARP or FLAG-tagged TGF-β1, TGF-β2, or TGFβ3 pro-forms was detected by flow cytometry. Histograms are representative of triplicate transfectants in the same experiment. Inset numbers show mean ± SEM of mean fluorescence intensity. **B** and **C,** Immunoprecipitation followed by Western blotting. Expi293F cells were transfected with plasmids encoding LRRC33 (L), TGFβ1 (T1), TGFβ2 (T2), or TGFβ3 (T3) pro-forms as in **A**. Cell lysates were subjected to (**B**) reducing or (**C**) nonreducing SDS-PAGE either directly or after IP and then WB as shown under images. **B** and **C,** Blank spaces: separate lanes from the same gel that were imaged together and then moved. Results are representative of two independent experiments.

metastatic nodules on the lung surface than WT mice (**Fig. 2G** and **H**). More definitive quantitation using hematoxylin and eosin staining of lung tissue sections showed an 82% decrease in metastasis in *Lrrc33*$^{-/-}$ mice compared with WT mice (**Fig. 2I** and **J**). Heterozygous mice also showed significantly decreased lung metastasis (**Fig. 2G–J**). Overall, our observations showed that loss of LRRC33 slowed tumor growth in three cancer types that vary in immunogenicity, including highly immune-infiltrated MC38 tumors and less-infiltrated B16.F10 and LLC1 tumors, and significantly reduced melanoma lung metastasis.

We next investigated whether loss of LRRC33 abolished pro-TGFβ1 expression on tumor-associated myeloid cells. TGFβ1 prodomain staining and flow cytometry showed that Mac-1$^+$F4/80$^+$ macrophages, Mac-1$^+$CD11c$^+$ DCs, and Mac-1$^+$Gr-1$^+$ MDSCs isolated from *Lrrc33*$^{-/-}$ B16.F10 tumors lacked cell surface pro-TGFβ1 although staining of MDSCs was weak (**Fig. 3A**). Similar results were obtained with myeloid cells isolated from MC38 tumors (**Fig. 3B**). After permeabilization, pro-TGFβ1 was detected, suggesting that pro-TGFβ1 was still present inside cells with LRRC33 deficiency (**Fig. 3B**), in agreement with what has been observed in peritoneal macrophages (16) and in transfectants coexpressing human patient LRRC33 mutants and TGFβ1 (26).

Loss of cell surface TGFβ1 correlates with loss of activatable TGFβ1 in tumor-associated myeloid cells

Myeloid cell populations were purified from MC38 tumors harvested from WT and *Lrrc33*$^{-/-}$ mice by negative and positive antibody panning. Cell purity was verified by flow cytometry (**Fig. 3C**). Cells were cocultured with CAGA cells, a TGFβ reporter cell line, in the presence or absence of integrin αVβ6-transfected Expi293F cells. Total Mac-1$^+$ myeloid cells, as well as macrophages, DCs, and MDSCs, from tumors in WT mice produced activated TGFβ1, whereas this was not seen with the same cell types isolated from MC38 tumors in *Lrrc33*$^{-/-}$ mice (**Fig. 3D**). Activation was dependent on integrin αVβ6. Total Mac-1$^+$ myeloid cells, macrophages, and DCs isolated from *Lrrc33*$^{-/-}$ bone marrow also lacked activatable TGFβ (**Fig. 3E**). Comparison of pro-TGFβ1 expression and activatable TGFβ on bone marrow and tumor-infiltrating myeloid cells showed that cells from heterozygous *Lrrc33*$^{+/-}$ mice were consistently intermediate between cells from WT and KO mice, although not significantly different compared with cells from WT mice (Supplementary Fig. S2).

Loss of LRRC33 biases tumor-infiltrating immune cells toward a more activated phenotype

To investigate the cellular mechanisms connecting loss of LRRC33-dependent TGFβ1 activation to slower tumor growth, we phenotyped MC38 tumor-infiltrating leukocytes 14 days after subcutaneous tumor cell injection. Although CD45$^+$ immune cell infiltration did not significantly change, CD3$^+$ and CD8$^+$ T cells, as well as NK1.1$^+$ NK cells, were significantly increased in *Lrrc33*$^{-/-}$ compared with WT mice, including both as frequency among CD45$^+$ cells (**Fig. 4A** and **B**) and per mg of tumor (Supplementary Fig. S3). In contrast, LRRC33 loss did not significantly affect CD4$^+$ T-cell frequency or number. Although Tregs express GARP/TGFβ1 complexes and are regulated by TGFβ1 (13), we did not see a significant difference of tumor Treg

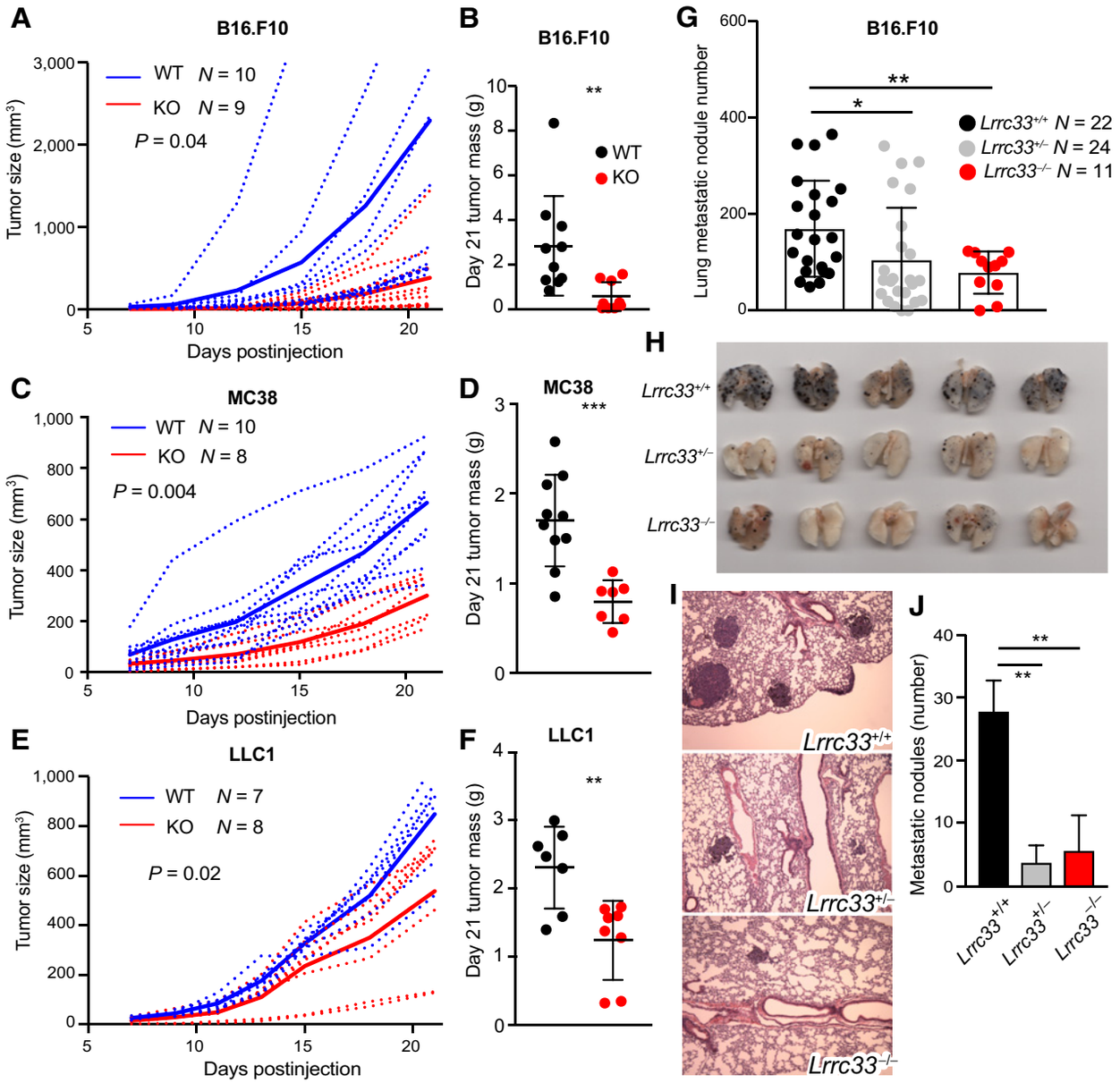

Figure 2.

LRRC33 deficiency decreases syngeneic tumor growth and metastasis. **A–F,** Tumor growth after (**A**, **B**) 1×10^5 B16.F10; (**C**, **D**) 3×10^5 MC38; or (**E**, **F**) 1×10^4 LLC1 cells were subcutaneously injected into the right flank of WT and *Lrrc33*$^{-/-}$ (KO) mice. Dashed and solid lines: individual animals and group average, respectively. *P* values are for the last time point, as determined by unpaired Student *t* test. **G–J,** B16.F10 melanoma lung metastasis. B16.F10 cells (3×10^5) were intravenously injected into *Lrrc33*$^{+/+}$, *Lrrc33*$^{+/-}$, or *Lrrc33*$^{-/-}$ mice. Metastases were counted 14 days later. **G** and **H,** Lung metastases were counted by gross observation after perfusion. **I** and **J,** H&E staining (10× magnification) to quantitate metastatic lesions as the average number per six whole-lung sections (5 mice/group). Data show mean ± SEM. *, $P < 0.05$; **, $P < 0.01$; ***, $P < 0.001$, as determined by unpaired Student *t* test. Results are representative of two or more independent experiments.

infiltration between tumors from WT and *Lrrc33*$^{-/-}$ mice (**Fig. 4C** and **D**). We also evaluated myeloid cell subsets. The proportions of Mac-1$^+$CD11c$^+$ DCs and Mac-1$^+$F4/80$^+$ macrophages were not significantly different between *Lrrc33*$^{-/-}$ and WT mice (**Fig. 4B**). Tumor-associated macrophages (TAM) were not skewed significantly into MHCII$^+$CD206$^-$ (M1-like) or MHCII$^-$CD206$^+$ (M2-like) phenotypes (**Fig. 4E** and **F**). However, the proportion of CD11b$^+$Gr-1$^+$ MDSCs was significantly decreased in *Lrrc33*$^{-/-}$ mice (**Fig. 4B**).

We next asked whether the increase in CD8$^+$ T cells and NK cells in *Lrrc33*$^{-/-}$ mice was accompanied by enhancement of functional activity. CD8$^+$ T cells showed significant increases in the proportion of TNFα$^+$, IFNγ$^+$, and granzyme B$^+$ cells in tumors from *Lrrc33*$^{-/-}$ mice, including a ∼2-fold increase in TNFα-secreting cells

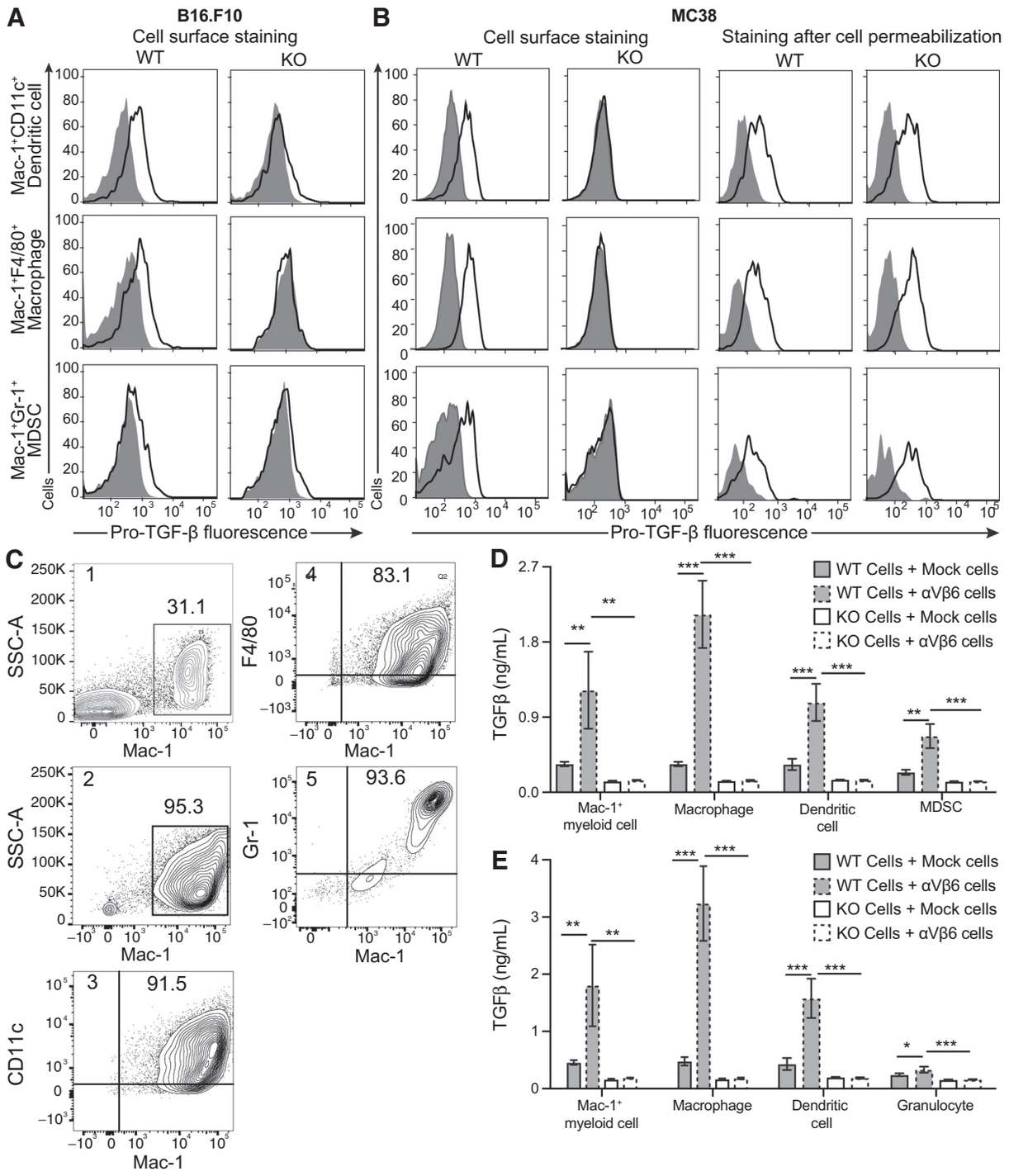

Figure 3.

Lrrc33$^{-/-}$ tumor-associated myeloid cells lack cell surface pro-TGFβ1 expression and activation. **A** and **B,** Pro-TGFβ1 expression was measured 14 days after subcutaneous (**A**) B16.F10 and (**B**) MC38 cell injection. Tumors were harvested and dissociated to obtain single-cell suspensions, and cells were analyzed for the indicated markers. Surface and intracellular pro-TGFβ1 was assessed for the indicated immune cell populations by flow cytometry. Gray filled histograms and black curves show control antibody and anti-pro-TGFβ1 staining, respectively. Flow cytometry results were similar for cells from 3 mice/group, and one representative is shown for each. **C,** Mac-1^{+} myeloid cells from (1) whole bone marrow were purified by (2) antibody panning and (3) further panned to isolate DCs, (4) macrophages, and (5) granulocytes. **D** and **E,** Myeloid cell populations were purified (as in **C**) from (**D**) MC38 tumor or (**E**) bone marrow and cocultured with CAGA cells in the presence of mock or αVβ6-transfected Expi293F cells and assayed for TGFβ production. Data show mean ± SEM of quadruplicate samples. *, $P < 0.05$; **, $P < 0.01$; ***, $P < 0.001$, as determined by unpaired Student *t* test. Results in **A**–**D** are representative of two to three independent experiments.

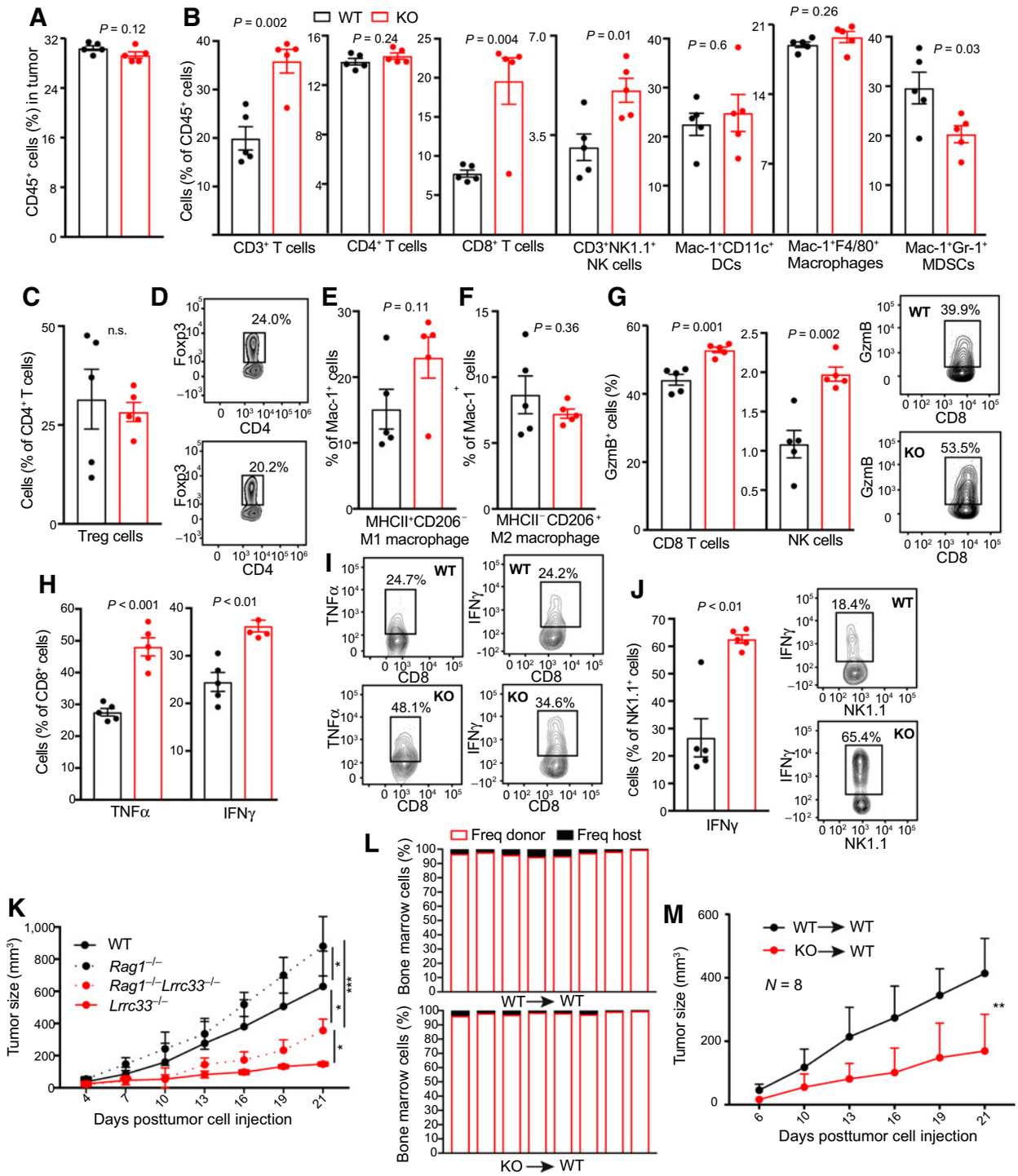

Figure 4.

LRRC33 deficiency in hematopoietic cells augments both innate and adaptive host immune responses to MC38 tumors. **A–J,** Phenotype of tumor-filtrating immune cells 14 days after subcutaneous MC38 injection in WT or *Lrrc33* KO mice. Cells from tumors were stained for the indicated markers and subjected to flow cytometry from five mice/group (one sample of IFNγ-stained cells was lost in **H**). Mean ± SEM is shown. *P* values were determined by unpaired Student *t* test. Representative flow cytometry profiles for one sample from WT and KO mice are shown in (**D**, **G**, **I**, and **J**). Overall results are representative of two independent experiments. GzmB, granzyme B. **K,** Effect of *Rag1* and *Lrrc33* deficiency on MC38 tumor growth. Data show mean ± SEM for $n = 6–7$ mice. **L** and **M,** Tumor growth in WT mice transplanted with WT or *Lrrc33*$^{-/-}$ bone marrow cells. **L,** Whole bone marrow transplantation chimerism in individual mice. **M,** Growth of MC38 tumors in transplant recipients. Data show mean ± SEM for $n = 8$ mice/group. In **K**, **M**, *P* values are for the last time point, unpaired Student *t* test: *, $P < 0.05$; **, $P < 0.01$; ***, $P < 0.001$.

(**Fig. 4G–I**). Tumor-infiltrating granzyme B^+ NK cells were also significantly increased in *Lrrc33*$^{-/-}$ mice (**Fig. 4G**), along with an increase in the proportion of tumor-infiltrating IFNγ$^+$ NK cells, which increased from 26.7±14.0% in WT to 62.6±3.1% in *Lrrc33*$^{-/-}$ mice (**Fig. 4J**).

Experiments in a *Rag1*$^{-/-}$ background showed that tumors grew significantly faster in *Lrrc33*$^{-/-}$*Rag1*$^{-/-}$ mice than in *Lrrc33*$^{-/-}$ mice, demonstrating that deficiency of LRRC33 augmented specific immune responses (**Fig. 4K**). This increase in growth rate was comparable with the faster growth in *Rag1*$^{-/-}$ mice compared with WT mice. MC38 tumors were also significantly smaller in *Lrrc33*$^{-/-}$*Rag1*$^{-/-}$ mice than in *Rag1*$^{-/-}$ mice, indicating that deficiency of LRRC33 also augmented innate immunity. Immunophenotyping showing increased TNFα$^+$, IFNγ$^+$, and granzyme B^+ $CD8^+$ T cells is consistent with increased adaptive immunity, whereas higher infiltration of IFNγ$^+$ and granzyme B^+ NK cells are likely to contribute to the higher innate immunity in *Lrrc33*$^{-/-}$ mice (**Fig. 4G–J**). To test the contribution of hematopoietic cells to the effects on tumor growth, we transferred CD45.2$^+$ WT or *Lrrc33*$^{-/-}$ whole bone marrow cells to lethally irradiated CD45.1$^+$ WT mice. Chimerism was greater than 95% at 10 weeks (**Fig. 4L**). Chimeric mice that received *Lrrc33*$^{-/-}$ bone marrow exhibited significantly slower MC38 tumor growth than mice that received WT bone marrow (**Fig. 4M**).

Because immune responses vary among tumors, we extended examination of tumor-infiltrating leukocytes to the subcutaneous B16.F10 melanoma model (**Fig. 5A** and **B**; Supplementary Fig. S4). $CD8^+$ T cells were significantly increased in tumor infiltrates in *Lrrc33*$^{-/-}$ compared with WT mice. $CD8^+$ T cells also showed significant increases in the proportion of cells expressing TNFα, IFNγ, and granzyme B, ranging from 1.7- to 2.7-fold (**Fig. 5C** and **D**). In contrast to results with $CD8^+$ T cells and results with NK cells in MC38 tumors, NK1.1$^+$ NK cells infiltrating B16.F10 tumors showed no increase in expression of IFNγ and granzyme B (**Fig. 5E**). Numbers of Mac-1$^+$CD11c$^+$ DCs and Mac-1$^+$F4/80$^+$ macrophages infiltrating B16.F10 tumors showed no differences between WT and *Lrrc33*$^{-/-}$ mice (**Fig. 5F**). However, macrophages were skewed in phenotype. MHCII$^+$CD206$^-$ (M1-like) TAMs were significantly increased and MHCII$^-$CD206$^+$ (M2-like) were significantly decreased in *Lrrc33*$^{-/-}$ mice (**Fig. 5G** and **H**). In summary, in B16.F10 melanoma, LRRC33 deficiency polarized immune cells toward a more immune reactive phenotype, as in MC38 carcinomas, yet there were also differences from MC38 among T-cell, NK-cell, and macrophage subpopulations in the way they were skewed.

Although immune cell populations are reported to be normal in *Lrrc33*$^{-/-}$ mice (20), we evaluated immune cell subsets to test if any of the skewing seen in tumor-infiltrating cells was preexisting in tumor-free mice (Supplementary Fig. S5). Compared with WT mice, *Lrrc33*$^{-/-}$ mice had comparable percentages of splenic $CD3^+$, $CD4^+$, and $CD8^+$ T cells, B cells, NK cells, Mac-1$^+$F4/80$^+$ macrophages, Mac-1$^+$CD11c$^+$ DCs, and Mac-1$^+$Gr-1$^+$ granulocytes (Supplementary Fig. S5A). Intracellular functional markers (granzyme B and IFNγ) in splenic $CD8^+$ T cells and NK cells also showed no significant differences (Supplementary Figs. S5B–S5D). *Lrrc33* loss did not significantly affect Ly6C$^+$ monocytes nor Ly6G$^+$ polymorphonuclear (PMN) neutrophils among splenic Mac-1$^+$ cells (Supplementary Figs. S5E and S5F). Thymus $CD4^+CD8^-$, $CD4^-CD8^-$, $CD4^-CD8^+$, and $CD4^+CD8^+$ T-cell also showed no difference between WT and KO mice (Supplementary Figs. S5G and S5H). However, in lungs, although extravascular innate and adaptive immune cells in *Lrrc33*$^{-/-}$ mice were otherwise normal, there was a significant decrease in $CD103^{high}CD11c^+CD11b^-MHCII^+$ DCs (Supplementary Figs. S5I and S5J). This finding may relate to the unusual susceptibility of *Lrrc33*$^{-/-}$ mice to pneumonia and otitis media (16). *Lrrc33* mRNA is selectively expressed on immune cells and tumors, and LRRC33 has only been found on immune cells (16, 20, 34). We therefore assessed expression in B16.F10 tumor cells. *Lrrc33* mRNA was not expressed on B16.F10 tumor cells grown *in vivo* (Supplementary Fig. S6).

LRRC33 deficiency, TGFβ antibody treatment, and inhibition of SMAD phosphorylation

We next compared deficiency of LRRC33 to inhibition of TGFβ signaling using the 21D1 antibody, which reacts with the growth factor moiety of TGFβ1 with a K_d of <0.5 pmol/L and with that of TGFβ3 with a K_d of 4.9 nmol/L (29). Blocking TGFβ signaling led to significantly stronger inhibition of MC38 tumor growth in WT mice than deficiency of LRRC33 (Fig. 6A). Moreover, 21D1 antibody inhibited MC38 tumor growth to similar extents in *Lrrc33*$^{-/-}$ and WT mice. Similar results were obtained with B16.F10 tumors, with tumor growth being inhibited similarly in WT and *Lrrc33*$^{-/-}$ mice (**Fig. 6B**). These results suggest that TGFβ from sources other than LRRC33/TGFβ1 complexes, including complexes of LTBP and GARP with TGFβ1 or TGFβ3 from host or tumor cells, also contribute to tumor growth.

To test for TGF-β production by B16.F10 and MC38 cells, we co-cultured them *in vitro* with CAGA indicator cells. Both cell lines produced active TGF-β (**Fig. 6C** and **D**), and the majority of TGF-β was neutralized by 50 nmol/L 21D1 antibody (**Fig. 6E** and **F**). Essentially identical results were obtained with mock and integrin αVβ6-transfected Expi293F cells. Because we used purified TGFβ1 to standardize our assays, we calculated that in our assays, B16.F10 and MC38 cells secreted about 3×10^{-4} and 11×10^{-4} pg/cell of TGFβ1 equivalents, respectively, whereas the myeloid cells in MC38 tumors secreted on average 6×10^{-4} pg/cell. The caveat to these calculations is that although there was a dose–response relationship between the number of tumor cells and TGFβ production, the relationship was not linear (the intermediate cell number in **Fig. 6C** and **D** was used for calculations). qRT-PCR showed high expression of TGFβ1 and less expression of TGFβ3 mRNA in B16.F10 and MC38 cells, less TGFβ2 mRNA in B16.F10 cells, and almost no TGFβ2 mRNA in MC38 cells (**Fig. 6G** and **H**).

Although TGFβ is known to directly act on adaptive and innate immune cells in the TME (1), we verified this in the MC38 tumor model using *Lrrc33*$^{-/-}$ mice by measuring intracellular phosphorylated SMAD2 and SMAD3 (pSMAD2/3). SMAD2/3 phosphorylation was decreased in MC38 tumors in *Lrrc33*$^{-/-}$ mice compared with WT in immune cells, particularly in $CD3^+$ and NK cells (**Fig. 6I** and **J**). Decreased pSMAD2/3 was seen in tumor-infiltrating CD45$^+$, $CD3^+$, Mac-1$^+$, and NK populations in *Lrrc33*$^{-/-}$ mice at all timepoints measured (days 7, 14, and 21) and reached significance in at least one timepoint for each population (**Fig. 6J**). There was no significant change in pSMAD2/3 in either tumor epithelial cells or fibroblasts (**Fig. 6J**). We also compared the effect of the 21D1 antibody to TGFβ1 and β3 on SMAD2/3 phosphorylation 7 days after beginning treatment. Treatment reduced TGFβ signaling in CD45$^+$ immune cells and CD45$^-$ nonimmune cells alike in MC38 tumors (**Fig. 6K** and **L**). In contrast, *Lrrc33* deficiency was completely selective, whereby it reduced TGFβ signaling only in immune cells.

LRRC33-deficiency enhances anti-PD-1 efficacy in the B16.F10 model

B16.F10 tumors are immune checkpoint therapy-resistant (35, 36), in agreement with lack of a significant effect of PD-1 antibody in WT

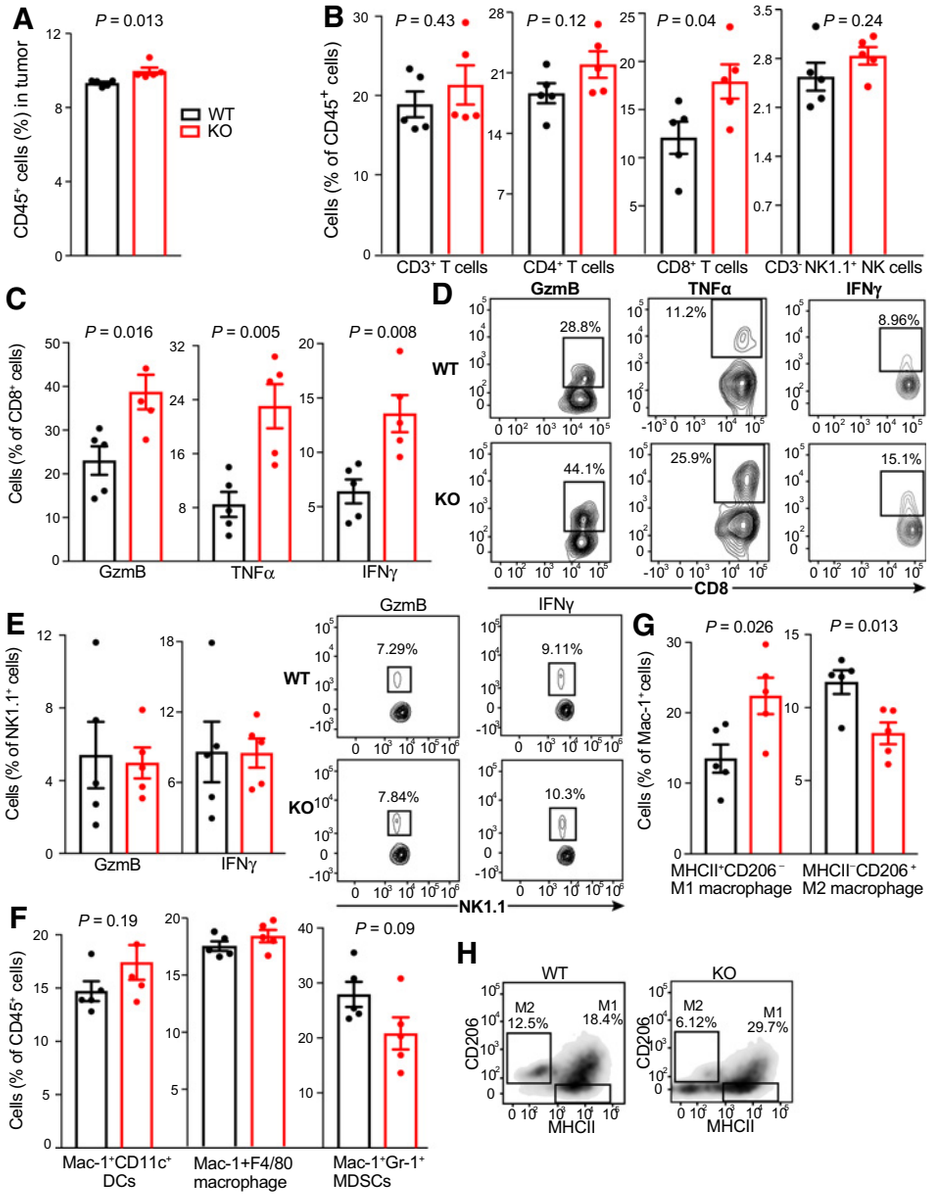

Figure 5.

Slower growth of B16.F10 tumors in *Lrrc33* KO mice associates with increased infiltration of effector cells and altered macrophage phenotype. **A–H,** Phenotype of tumor-filtrating immune cells 14 days after subcutaneous B16.F10 injection. The indicated immune populations were measured by flow cytometry in tumors from five mice/group; mean ± SEM. Representative flow cytometry profiles for one sample from WT and KO mice are shown in **D**, **E**, and **H**. *P* values were determined by unpaired Student *t* test. Data are representative of two independent experiments.

mice (**Fig. 7A**). However, treating *Lrrc33*$^{-/-}$ mice with PD-1 antibody significantly reduced B16.F10 tumor growth (**Fig. 7A**). Tumor size reduction persisted throughout the experiment and was synergistic (combined treatments reduced tumor size more than the sum of the two treatments). Contrasting results were obtained in the PD-1–sensitive MC38 colon carcinoma model (37), in which PD-1 blockade more strongly inhibited MC38 tumor growth than *Lrrc33* deficiency (**Fig. 7B**).

To provide mechanistic insights into how loss of LRRC33-sensitized B16.F10 melanoma to anti-PD-1 treatment, we examined tumor-infiltrating leukocytes by flow cytometry. PD-1 blockade in WT mice did not affect infiltration by CD45$^+$, CD3$^+$, CD4$^+$, CD8$^+$, and NK cells in tumors (**Fig. 7C–E**). However, the combination of PD-1 blockade with LRRC33 deficiency led to an increase in tumor-infiltrating CD3$^+$ and CD8$^+$ T cells, as well as NK cells, and the increase with the combination was often significant compared with either alone (**Fig. 7D**). Furthermore, the combination significantly increased granzyme B CD8$^+$ T cells and NK cells relative to deficiency or treatment in WT mice (**Fig. 7E** and **F**). TNFα was similarly increased in CD8$^+$ T cells by anti-PD-1 plus LRRC33 deficiency and was significantly increased in the combination relative to either deficiency or treatment alone (Fig. 7F). Moreover, IFNγ in both tumor-infiltrating NK cells and CD8$^+$ cells were increased with deficiency and treatment and were significantly augmented by the combination of LRRC33 deficiency and PD-1 treatment relative to either alone (**Fig. 7E** and **F**). These data suggest that loss of LRRC33-dependent TGFβ1 activity potentiates the ability of anti-PD-1 to enhance antitumor immunity by increasing immigration of CD8 and NK cells and enhancing their effector activity.

Myeloid cell infiltration was also affected by treatment. Blockade of PD-1 in *Lrrc33*$^{-/-}$ mice significantly increased infiltration of DCs

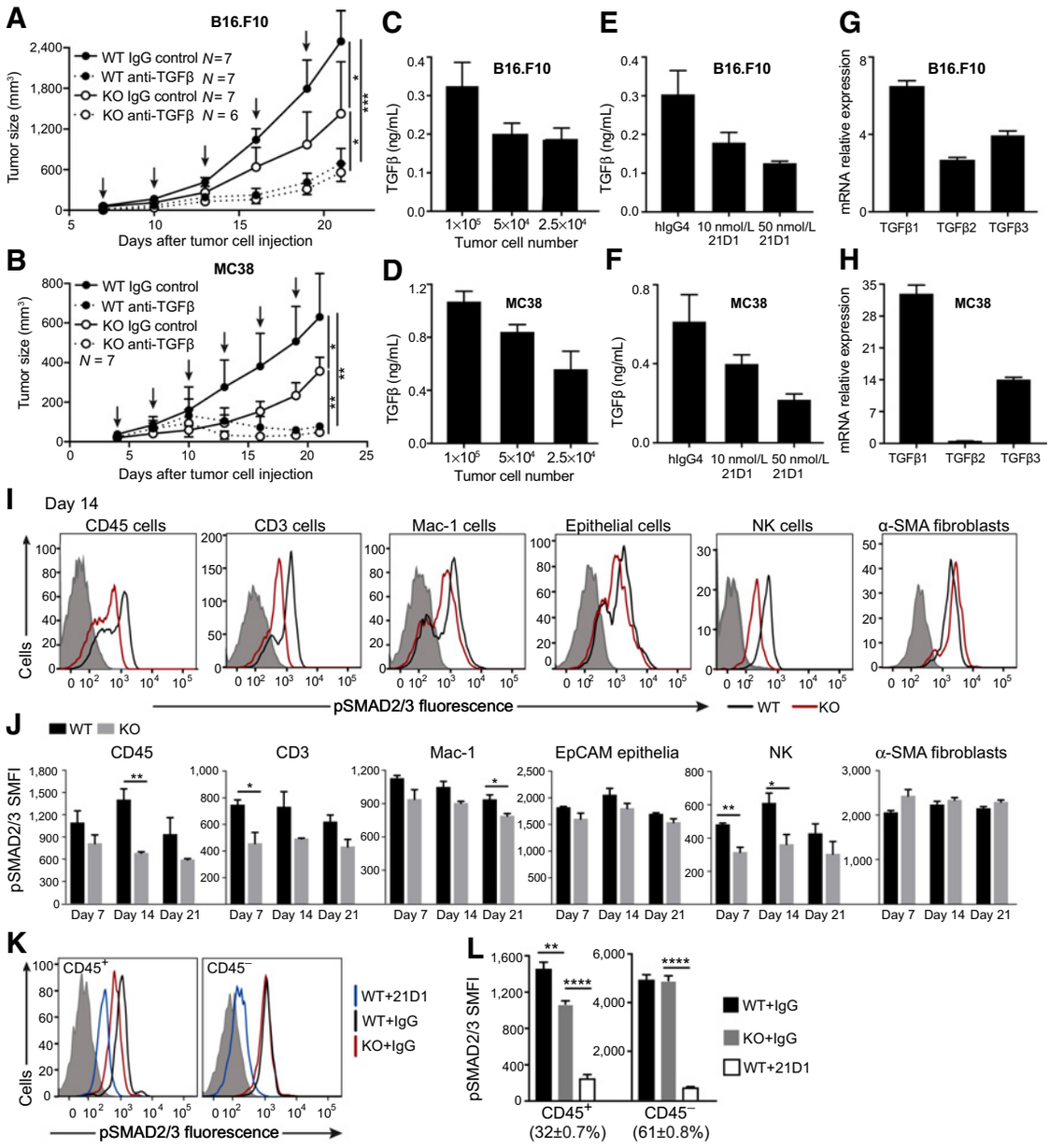

Figure 6.

Blocking TGFβ1 with an antibody inhibits tumor growth and pSMAD2/3 signaling more effectively than LRRC33 deficiency. **A** and **B,** Effect of TGFβ antibody 21D1 (specific for the TGFβ1 and TGFβ3 growth factors) on growth of (**A**) B16.F10 and (**B**) MC38 tumors in WT or *Lrrc33*$^{-/-}$ mice. Mice were treated with 10 mg/kg 21D1 antibody or isotype control on indicated days (arrows) after tumor cell subcutaneous injection. Data show mean ± SEM for $n = 6$–7 mice. *P* values are shown for last time point, unpaired Student *t* test (*, $P < 0.05$; **, $P < 0.01$; ***, $P < 0.001$). **C–H,** TGFβ release and mRNA expression in (**C**, **E**, **G**) B16.F10 and (**D**, **F**, **H**) MC38 tumor cells. **C** and **D,** TGFβ release from the indicated number of tumor cells measured by co-culture with CAGA cells in the presence of mock-transfected Expi293F cells for 24 hours. Data are mean ± SEM of quadruplicate samples. **E** and **F,** Effect of 21D1 or IgG4 control antibody (50 nmol/L) on TGFβ production by tumor cells (1×10^5) co-cultured with CAGA cells for 24 hours. Data are mean ± SEM of quadruplicate samples. **G** and **H,** *Tgfb1*, *Tgfb2*, and *Tgfb3* mRNA expression relative to *Gapdh* in B16.F10 and MC38 cell lines determined by qRT-PCR. Expression determined using the $2^{-\Delta Ct}$ method is presented as mean ± difference of duplicates. Data are representative of two independent experiments. **I** and **J,** Phosphorylated (p)SMAD2/3 in immune cells and nonimmune cells in MC38 tumors from WT and *Lrrc33*$^{-/-}$ mice measured by flow cytometry. **I,** pSMAD2/3 expression in the indicated cell types in one representative tumor from WT and *Lrrc33*$^{-/-}$ mice on day 14. Control antibody: gray histogram; WT: black curve; KO: red curve. **J,** pSMAD2/3 expression in tumors from $n = 3$ mice/group on day 7, 14, and 21 after tumor injection (mean ± SEM). SMFI: specific mean fluorescence intensity (after isotype control subtraction). **K** and **L,** pSMAD2/3 expression measured by flow cytometry in MC38 tumors 7 days after treatment of WT mice with 21D1 antibody or treatment of WT or KO mice with IgG4 control antibody. **K,** Representative histograms of staining with anti-pSMAD2/3 in the indicated groups. WT+21D1: blue curve; KO+IgG: red curve; WT+IgG: black curve; isotype control staining: gray-shaded histogram. **L,** pSMAD2/3 SMFI of CD45$^+$ and CD45$^-$ cells in 4 mice/group, mean ± SEM. The % of CD45$^+$ and CD45$^-$ cells in tumors is also shown (*, $P < 0.05$; **, $P < 0.01$; ***, $P < 0.001$; ****, $P < 0.0001$, as determined by unpaired Student *t* test).

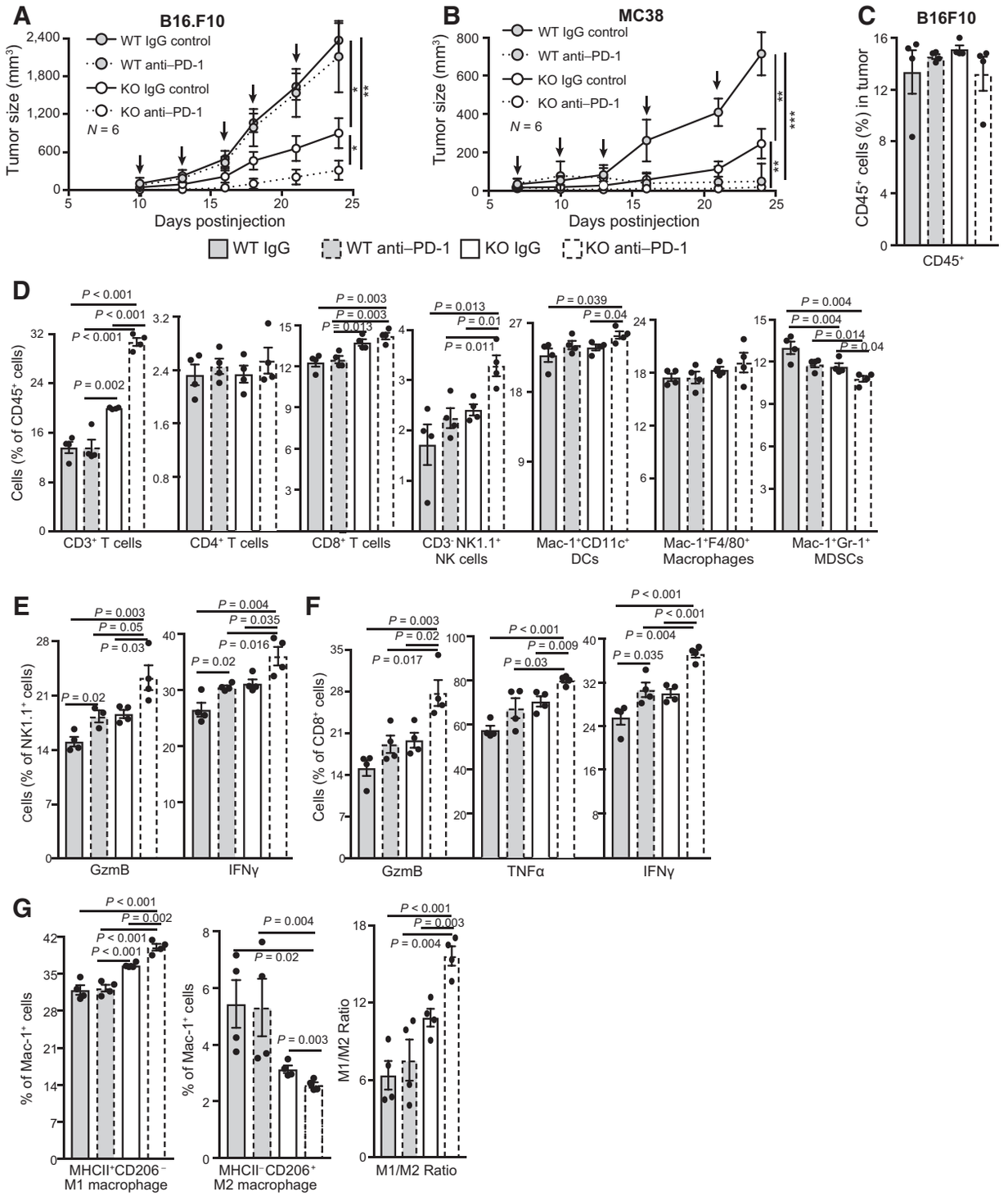

Figure 7.

LRRC33 loss and PD-1 blockade synergize in controlling B16.F10 tumor growth by altering the tumor immune landscape. **A** and **B,** Growth of (**A**) B16.F10 and (**B**) MC38 tumors injected subcutaneously in WT and KO mice treated intraperitoneally with 10 mg/kg of anti-PD-1 or IgG control antibody on indicated days (arrows). Data are mean ± SEM for $n = 6$ mice. *P* values are for the last time point, unpaired Student *t* test; *, $P < 0.05$; **, $P < 0.01$; ***, $P < 0.001$. Data are representative of two independent experiments. **C–G,** Mice (4/group) were injected subcutaneously with B16.F10 cells and treated with antibodies as in **A** on days 7, 10, and 13 and sacrificed on day 15 for flow cytometric analysis of immune cell populations in tumors. Mean ± SEM is shown. *P* values were determined by unpaired Student *t* test.

(**Fig. 7D**). Furthermore, MDSCs were decreased by LRRC33 deficiency and PD-1 treatment and further decreased by their combination (**Fig. 7D**). Phenotyping macrophages for CD206 and MHCII expression showed that LRRC33 deficiency had a more significant effect than anti-PD-1 in both increasing the $MHCII^+CD206^-$ M1 population and decreasing the $MHCII^-CD206^+$ M2 population (**Fig. 7G**). However, skewing towards M1 was significantly enhanced by addition of anti-PD-1 to LRRC33 deficiency (**Fig. 7G**). Overall, the results suggest that LRRC33 deficiency leads to a more immunogenic B16.F10 TME and improved anti-PD-1 efficacy. These data emphasize the therapeutic potential of dual blockade of LRRC33/TGFβ1 and PD-1 in cancer immunotherapy.

Discussion

Here, we focused on a selective approach to tumor therapy: inhibiting only one (of many combinations) of the three TGFβ isoforms associated with their five well-characterized milieu molecules, LTBP1, 3, and 4, GARP, and LRRC33 (16, 18). We used this approach because in contrast to *Tgfb1*$^{-/-}$ mice, *Lrrc33*$^{-/-}$ mice show no autoimmune or inflammatory disease (16, 20). We confirmed here, and extended to further myeloid cell types, that LRRC33 associates with TGFβ1 and is required for TGFβ1 expression and activation (16, 34). GARP has been known only to associate with TGFβ1 (38–40). Here, we showed that GARP associated with and presented all three TGFβ isoforms on the cell surface, whereas LRRC33 only productively interacted with TGFβ1. This is the first time that a milieu molecule has been shown to associate with a unique TGFβ1 isoform.

Tumors grew more slowly in *Lrrc33*$^{-/-}$ than in WT mice, which we traced to a lack of TGFβ1/LRRC33 complexes and activatable TGFβ1. B16.F10 lung metastasis was also decreased. Whole bone marrow transplantation confirmed that hematopoietic *Lrrc33*$^{-/-}$ cells were sufficient to slow tumor growth in WT mice, in agreement with the finding that TGFβ1/LRRC33 complexes were primarily expressed on myeloid cell types. Tumors in *Lrrc33*$^{-/-}$ mice showed increased infiltration of both adaptive immune $CD3^+$ and $CD8^+$ T cells and innate immune NK cells, TAMs were skewed toward an M1-like phenotype, and MDSC infiltration was decreased. In addition, $CD8^+$ T-cell and NK-cell effector phenotype was enhanced. These results are consistent with results from *Lrrc33*$^{-/-}$ and$^-$ *Rag1*$^{-/-}$ mouse crosses, which showed that *Lrrc33*$^{-/-}$ lowered tumor growth by increasing both adaptive and innate immune cell responses. Phosphorylation of SMAD2/3 was decreased in infiltrating adaptive and innate immune cells, demonstrating a direct effect of *Lrrc33* deficiency on TGFβ signaling in both immune arms (1). We confirmed that *Lrrc33*$^{-/-}$ deficiency did not affect immune cell subset distributions in spleen or thymus (20); however, we also found a reduction in the $CD103^{high}CD11c^+CD11b^-MHCII^+$ DC subset in lungs, which might be relevant to the predisposition of *Lrrc33*$^{-/-}$ mice to pneumonia (16). We observed synergy between *Lrrc33* deficiency and PD-1 blockade in slowing growth of checkpoint blockade-resistant B16.F10 tumors. These synergistic effects also contributed to increased infiltration of $CD8^+$ T cells and NK cells and their effector functions, and in skewing the M1/M2 macrophage subset ratio toward a more tumoricidal M1-like phenotype.

Our study suggests that TGFβ release from TGFβ1/LRRC33 complexes is localized at the cellular level within tumors. TGFβ1/β3 antibody, 21D1, more effectively inhibited tumor growth than *Lrrc33* deficiency. However, the inhibition of SMAD2/3 phosphorylation in tumor-infiltrating leukocytes by 21D1 was more dramatic compared with *Lrrc33* deficiency. Furthermore, SMAD2/3 phosphorylation in nonimmune cells in tumors was almost completely inhibited by 21D1 antibody and unaffected by *Lrrc33* deficiency. These results demonstrate the high selectivity of the TGFβ1 growth factor that is released from proTGFβ1/LRRC33 complexes within tumors for action on immune cells. As emphasized previously and demonstrated in the central nervous system, activation (release) of TGFβ1 takes place between an αVβ6 or αVβ8 integrin-bearing cell and a cell bearing proTGFβ1/LRRC33, and the released TGFβ acts on cells in the immediate proximity of its site of release (16). We did not identify the relevant integrin-expressing cells in our study; however, DCs are known to express integrin αVβ8 and antibodies to αVβ8 are effective at suppressing tumor growth (41). The selective effect of *Lrrc33* deficiency on non-LRRC33 bearing cells, including $CD3^+$, $CD8^+$, and NK cells, suggests that these cells are in close contact with TGFβ1/LRRC33-expressing myeloid cells in tumors, and that an αVβ6 or αVβ8 integrin-expressing cells may also be nearby. Notably, tumor-associated myeloid cells are one of the most important factors in suppressing immune responses to tumors and in inducing resistance to immune checkpoint blockade (42). Furthermore, DCs, macrophages, and MDSCs, all of which have activatable LRRC33/TGFβ1 complexes, accounted for 60% to 70% of the infiltrating leukocytes in this study.

Previous studies that combined inhibition of TGFβ1 or the TGFβ1/GARP complex with inhibition of PD-1 or PD-L1 showed substantial inhibition of tumor growth in mice and effects on tumor-infiltrating immune cells. Increases in $CD8^+$ T cells, decreases in M2-like macrophages, decreases in MDSCs, and a surprising increase in $Foxp3^+$ Tregs was found in one study (14), and increases in $CD8^+$ T cells were observed in other studies (5, 15). In contrast, combination TGFβ1/GARP and PD-1 blockade had no effect on tumor-infiltrating populations (13). However, this and two other studies report enhanced $CD8^+$ T-cell effectors (5, 13, 14). Our results were most different from TGFβ1/GARP blockade, suggesting that combination of TGFβ1/GARP and TGFβ1/LRRC33 could be additive or synergistic. We found here that $CD3^-$ NK cells, which were not examined in these previous studies, were increased in MC38 tumors in *Lrrc33*$^{-/-}$ mice and in B16.F10 tumors in *Lrrc33*$^{-/-}$ mice treated with PD-1 antibody.

Our results suggest that targeting the LRRC33 axis of TGFβ1 activation has promise as an immuno-oncology treatment strategy. It will be important to produce antibodies that specifically bind to the TGFβ1/LRRC33 complex and inhibit release of the active TGFβ1 growth factor, just as has been previously achieved for the TGFβ1/GARP complex (32, 43). Such antibodies would also allow overcoming two limitations of the current work: (i) the restriction of tumors to the C57BL/6 mouse strain carrying the *Lrrc33*$^{-/-}$ mutation and (ii) the inability to grow tumors prior to inhibiting the LRRC33 axis of TGFβ1 activation. Antibodies would also enable future translation to patients of the highly selective mechanism of inhibiting the LRRC33 axis of TGFβ1 activation in myeloid cells in the TME.

Authors' Disclosures

No disclosures were reported.

Authors' Contributions

A. Jiang: Conceptualization, investigation, visualization, methodology, writing–original draft. **Y. Qin:** Conceptualization, investigation, methodology, writing–review

and editing. **T.A. Springer:** Conceptualization, supervision, funding acquisition, visualization, project administration, writing–review and editing.

Acknowledgments

We thank Patricia Sousa for help with animal irradiation and whole bone marrow transplantation, the Arlene Sharpe lab for providing the MC38 cell line and consultation on tumor cell culture and injection, Colette Matysiak in the von Andrian Lab for assistance with lung immune cell staining and analysis, Chafen Lu for early work and advice, Vijay Kuchroo for advice, Roderick T. Bronson of the Rodent Pathology Core at Harvard Medical School, Wei Yang and Viet Le for critical comments on the manuscript, and Margaret Nielsen for illustrations. This work was supported by the NIH grant no. R01-HL159714 (to T.A. Springer).

The costs of publication of this article were defrayed in part by the payment of page charges. This article must therefore be hereby marked *advertisement* in accordance with 18 U.S.C. Section 1734 solely to indicate this fact.

Received July 21, 2021; revised November 22, 2021; accepted February 15, 2022; published first February 18, 2022.

References

1. Flavell RA, Sanjabi S, Wrzesinski SH, Licona-Limón P. The polarization of immune cells in the tumour environment by TGFβ. Nat Rev Immunol 2010;10:554–67.
2. Derynck R, Turley SJ, Akhurst RJ. TGFβ biology in cancer progression and immunotherapy. Nat Rev Clin Oncol 2020.
3. Colak S, Ten Dijke P. Targeting TGF-β signaling in cancer. Trends Cancer 2017;3:56–71.
4. Hugo W, Zaretsky JM, Sun L, Song C, Moreno BH, Hu-Lieskovan S, et al. Genomic and transcriptomic features of response to anti-PD-1 therapy in metastatic melanoma. Cell 2017;168:542.
5. Mariathasan S, Turley SJ, Nickles D, Castiglioni A, Yuen K, Wang Y, et al. TGFβ attenuates tumour response to PD-L1 blockade by contributing to exclusion of T cells. Nature 2018;554:544–8.
6. Tauriello DVF, Palomo-Ponce S, Stork D, Berenguer-Llergo A, Badia-Ramentol J, Iglesias M, et al. TGFβ drives immune evasion in genetically reconstituted colon cancer metastasis. Nature 2018;554:538–43.
7. Lan Y, Zhang D, Xu C, Hance KW, Marelli B, Qi J, et al. Enhanced preclinical antitumor activity of M7824, a bifunctional fusion protein simultaneously targeting PD-L1 and TGF-β. Sci Transl Med 2018;10:eaan5488.
8. Yang L, Huang J, Ren X, Gorska AE, Chytil A, Aakre M, et al. Abrogation of TGFβ signaling in mammary carcinomas recruits Gr-1+CD11b+ myeloid cells that promote metastasis. Cancer Cell 2008;13:23–35.
9. Pollard JW. Trophic macrophages in development and disease. Nat Rev Immunol 2009;9:259–70.
10. Yang L, DeBusk LM, Fukuda K, Fingleton B, Green-Jarvis B, Shyr Y, et al. Expansion of myeloid immune suppressor Gr+CD11b+ cells in tumor-bearing host directly promotes tumor angiogenesis. Cancer Cell 2004;6:409–21.
11. Marvel D, Gabrilovich DI. Myeloid-derived suppressor cells in the tumor microenvironment: expect the unexpected. J Clin Invest 2015;125:3356–64.
12. Gabrilovich DI, Ostrand-Rosenberg S, Bronte V. Coordinated regulation of myeloid cells by tumours. Nat Rev Immunol 2012;12:253–68.
13. de Streel G, Bertrand C, Chalon N, Lienart S, Bricard O, Lecomte S, et al. Selective inhibition of TGF-β1 produced by GARP-expressing Tregs overcomes resistance to PD-1/PD-L1 blockade in cancer. Nat Commun 2020;11:4545.
14. Martin CJ, Datta A, Littlefield C, Kalra A, Chapron C, Wawersik S, et al. Selective inhibition of TGFβ1 activation overcomes primary resistance to checkpoint blockade therapy by altering tumor immune landscape. Sci Transl Med 2020;12:eaay8456.
15. Dodagatta-Marri E, Meyer DS, Reeves MQ, Paniagua R, To MD, Binnewies M, et al. α-PD-1 therapy elevates Treg/Th balance and increases tumor cell pSmad3 that are both targeted by α-TGFβ antibody to promote durable rejection and immunity in squamous cell carcinomas. J Immunother Cancer 2019;7:62.
16. Qin Y, Garrison BS, Ma W, Wang R, Jiang A, Li J, et al. A milieu molecule for TGF-β required for microglia function in the nervous system. Cell 2018;174:156–71.
17. Hinck AP, Mueller TD, Springer TA. Structural biology and evolution of the TGF-β family. Cold Spring Harb Perspect Biol 2016;8:a022103.
18. Robertson IB, Rifkin DB. Regulation of the bioavailability of TGF-β and TGF-β-related proteins. Cold Spring Harb Perspect Biol 2016;8:a021907.
19. Su X, Mei S, Liang X, Wang S, Liu J, Zhang Y, et al. Epigenetically modulated LRRC33 acts as a negative physiological regulator for multiple Toll-like receptors. J Leukocyte Biol 2014;95:1–10.
20. Noubade R, Wong K, Ota N, Rutz S, Eidenschenk C, Valdez P, et al. NRROS negatively regulates reactive oxygen species during host defence and autoimmunity. Nature 2014;509:235–9.
21. Tsunawaki S, Sporn M, Ding A, Nathan C. Deactivation of macrophages by transforming growth factor-β. Nature 1988;334:260–2.
22. Wong K, Noubade R, Manzanillo P, Ota N, Foreman O, Hackney JA, et al. Mice deficient in NRROS show abnormal microglial development and neurological disorders. Nat Immunol 2017;18:633–41.
23. Butovsky O, Jedrychowski MP, Moore CS, Cialic R, Lanser AJ, Gabriely G, et al. Identification of a unique TGF-β-dependent molecular and functional signature in microglia. Nat Neurosci 2014;17:131–43.
24. Aluwihare P, Mu Z, Zhao Z, Yu D, Weinreb PH, Horan GS, et al. Mice that lack activity of αVβ6- and αVβ8-integrins reproduce the abnormalities of TGFβ1- and TGFβ3-null mice. J Cell Sci 2009;122:227–32.
25. Mobley AK, Tchaicha JH, Shin J, Hossain MG, McCarty JH. β8 integrin regulates neurogenesis and neurovascular homeostasis in the adult brain. J Cell Sci 2009;122:1842–51.
26. Dong X, Tan NB, Howell KB, Barresi S, Freeman JL, Vecchio D, et al. Bi-allelic LoF NRROS variants impairing Active TGF-β1 delivery cause a severe infantile-onset neurodegenerative condition with intracranial calcification. Am J Hum Genet 2020;106:559–69.
27. Smith C, McColl BW, Patir A, Barrington J, Armishaw J, Clarke A, et al. Biallelic mutations in NRROS cause an early onset lethal microgliopathy. Acta Neuropathol 2020;139:947–51.
28. Cash JN, Angerman EB, Kattamuri C, Nolan K, Zhao H, Sidis Y, et al. Structure of myostatin·follistatin-like 3: N-terminal domains of follistatin-type molecules exhibit alternate modes of binding. J Biol Chem 2012;287:1043–53.
29. Davies J, Dickinson CD, Marquis DM, Tang Y, Vaillancort PE, inventors; Eli Lilly and Company, Indianapolis, IN (US), assignee. Antibodies to TGF-β1. USA patent US 7,619,069 B2. 2009.
30. Oida T, Weiner HL. TGF-β induces surface LAP expression on murine CD4 T cells independent of Foxp3 induction. PLoS One 2010;5:e15523.
31. Kolodziej PA, Young RA. Epitope tagging and protein surveillance. Methods Enzymol 1991;194:508–19.
32. Cuende J, Lienart S, Dedobbeleer O, van der Woning B, De Boeck G, Stockis J, et al. Monoclonal antibodies against GARP/TGF-β1 complexes inhibit the immunosuppressive activity of human regulatory T cells in vivo. Sci Transl Med 2015;7:284ra56.
33. Novitskiy SV, Pickup MW, Chytil A, Polosukhina D, Owens P, Moses HL. Deletion of TGF-β signaling in myeloid cells enhances their anti-tumorigenic properties. J Leukoc Biol 2012;92:641–51.
34. Ma W, Qin Y, Chapuy B, Lu C. LRRC33 is a novel binding and potential regulating protein of TGF-β1 function in human acute myeloid leukemia cells. PLoS One 2019;14:e0213482.
35. Chen S, Lee LF, Fisher TS, Jessen B, Elliott M, Evering W, et al. Combination of 4-1BB agonist and PD-1 antagonist promotes antitumor effector/memory CD8 T cells in a poorly immunogenic tumor model. Cancer Immunol Res 2015;3:149–60.
36. Kleffel S, Posch C, Barthel SR, Mueller H, Schlapbach C, Guenova E, et al. Melanoma cell-intrinsic PD-1 receptor functions promote tumor growth. Cell 2015;162:1242–56.
37. Juneja VR, McGuire KA, Manguso RT, LaFleur MW, Collins N, Haining WN, et al. PD-L1 on tumor cells is sufficient for immune evasion in immunogenic tumors and inhibits CD8 T cell cytotoxicity. J Exp Med 2017;214:895–904.

38. Stockis J, Colau D, Coulie PG, Lucas S. Membrane protein GARP is a receptor for latent TGF-β on the surface of activated human Treg. Eur J Immunol 2009;39: 3315–22.
39. Tran DQ, Andersson J, Wang R, Ramsey H, Unutmaz D, Shevach EM. GARP (LRRC32) is essential for the surface expression of latent TGF-β on platelets and activated FOXP3+ regulatory T cells. Proc Natl Acad Sci U S A 2009;106:13445–50.
40. Wang R, Kozhaya L, Mercer F, Khaitan A, Fujii H, Unutmaz D. Expression of GARP selectively identifies activated human FOXP3+ regulatory T cells. Proc Natl Acad Sci U S A 2009;106:13439–44.
41. Dodagatta-Marri E, Ma HY, Liang B, Li J, Meyer DS, Chen SY, et al. Integrin αVβ8 on T cells suppresses anti-tumor immunity in multiple models and is a promising target for tumor immunotherapy. Cell Rep 2021;36:109309.
42. De Henau O, Rausch M, Winkler D, Campesato LF, Liu C, Cymerman DH, et al. Overcoming resistance to checkpoint blockade therapy by targeting PI3Kγ in myeloid cells. Nature 2016;539:443–7.
43. Lienart S, Merceron R, Vanderaa C, Lambert F, Colau D, Stockis J, et al. Structural basis of latent TGF-β1 presentation and activation by GARP on human regulatory T cells. Science 2018;362:952–6.

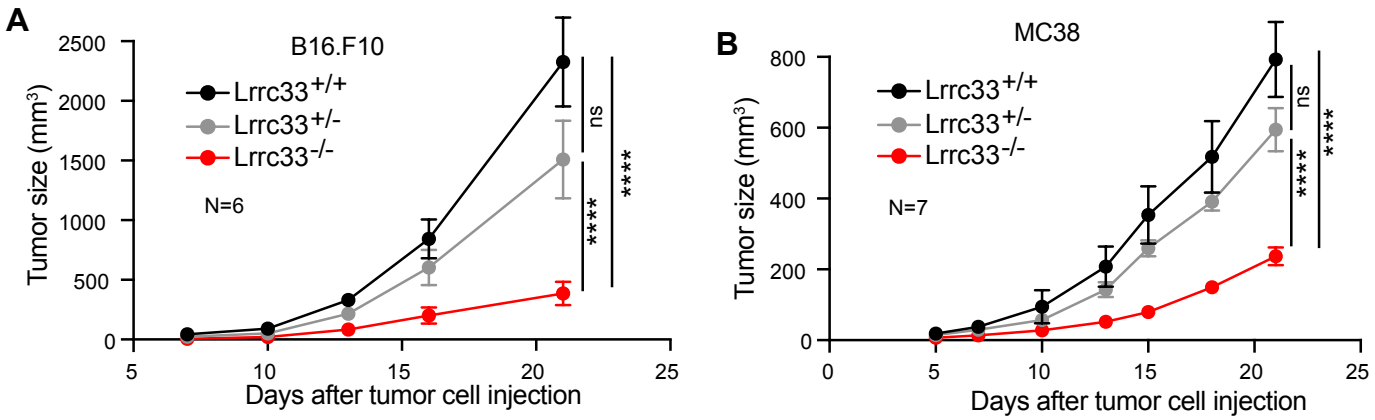

Supplementary Figure S1. *Lrrc33*$^{+/-}$ mice displayed slightly decreased tumor growth of B16F10 and MC38. B16F10 (A) or MC38 (B) cells were subcutaneously injected into the right flank of WT and KO mice. Data show mean ± SEM for n = 6 or 7 mice. P-values are determined by repeated measures two-way ANOWA including all the time points. * p<0.05, ** p<0.01, *** p<0.001, **** p<0.0001, ns, not significant.

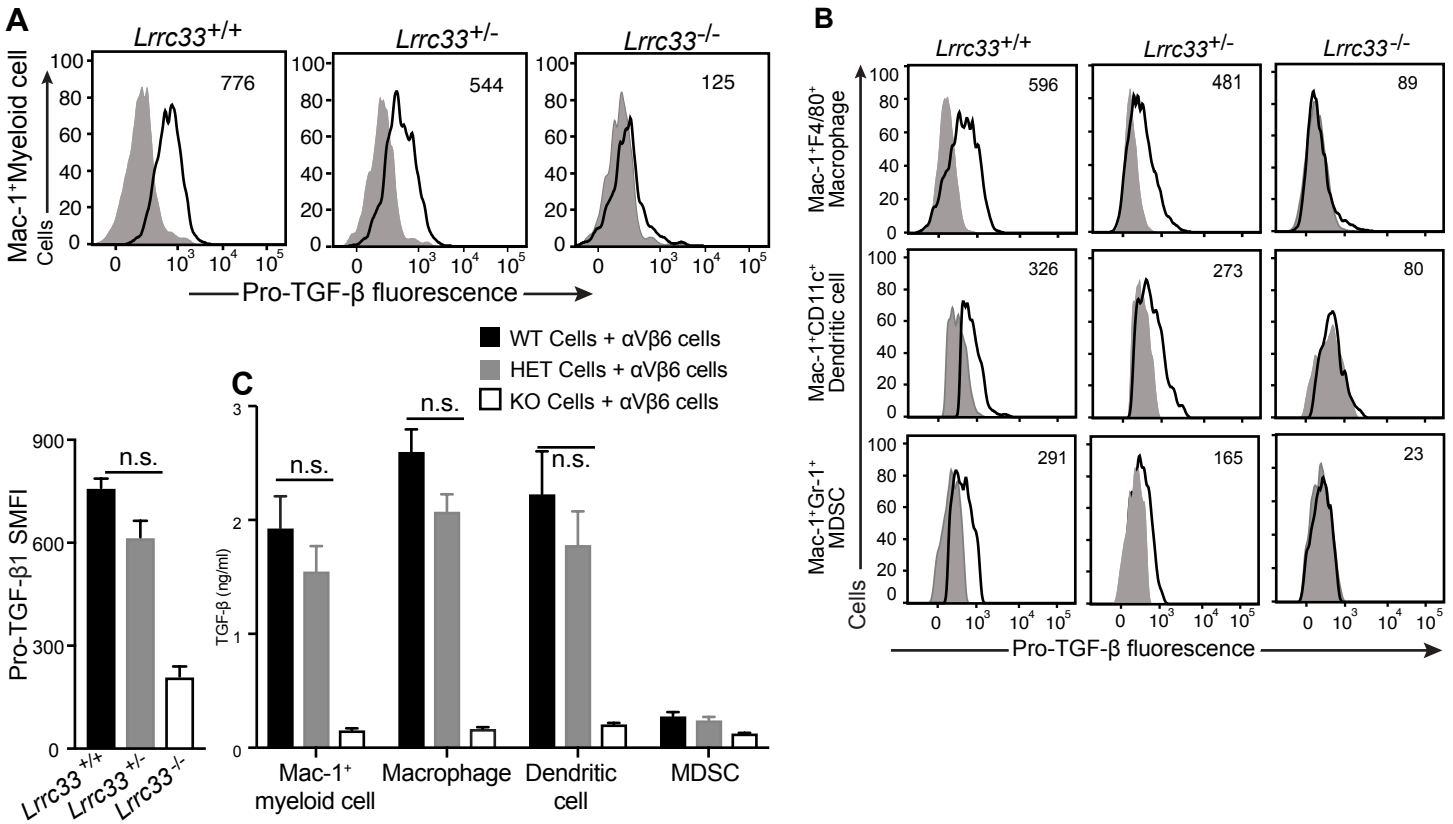

Supplementary Figure S2. *Lrrc33*$^{+/-}$ myeloid cells had slightly decreased cell surface pro-TGF-β1 expression and activation compared with WT cells. (A, B) Pro-TGF-β1 expression on bone marrow (A) and MC38 tumor (B) myeloid cell population was measured. Single-cells from bone marrow or tumor were stained with specific antibodies to characterize the indicated immune cell populations. Anti-pro-TGF-β1 or control antibody was then stained and analyzed by flow cytometry. Gray and black curve show control antibody and anti-pro-TGF-β 1 staining, respectively. Numbers show mean fluorescence intensity subtracted isotype control. **(C)** Indicated myeloid cell populations purified from MC38 tumors by antibody panning were co-cultured with CAGA cells in the presence of αVβ6-transfected Expi293F cells as described of Fig.2. 24 hours later, cell lysates were assayed for TGF-β measurement. Data show mean ± SEM of quadruplicate samples. n.s., not significant as determined by unpaired Student's t-test.

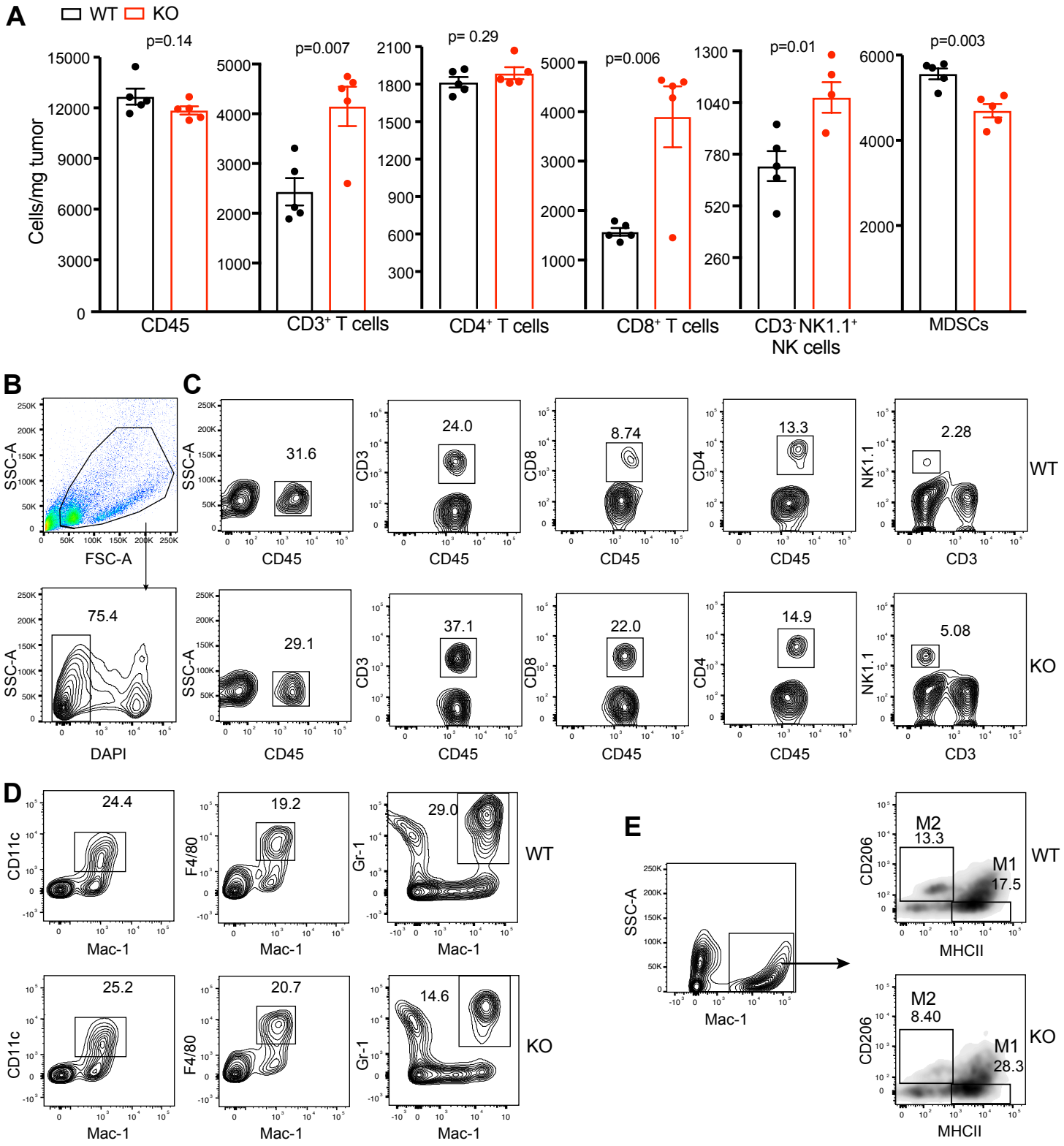

Supplementary Figure S3. MC38 tumor immune cell phenotyping. (A) Infiltrating cells were quantitated as numbers of cells per mg of tumor. Symbols show tumors from each of five mice per group. Results show mean ± SEM. P values were determined by unpaired Student's t-test. (B-D) Representative flow cytometry profiles for one sample from WT and KO mice. DAPI^{negative} live cells were gated from whole population, and CD45^{+} cells were gated from live cells for the subsequent analysis of indicated populations in C and D. (E) Representative flow cytometry profiles and gate strategy of M1 and M2 cells.

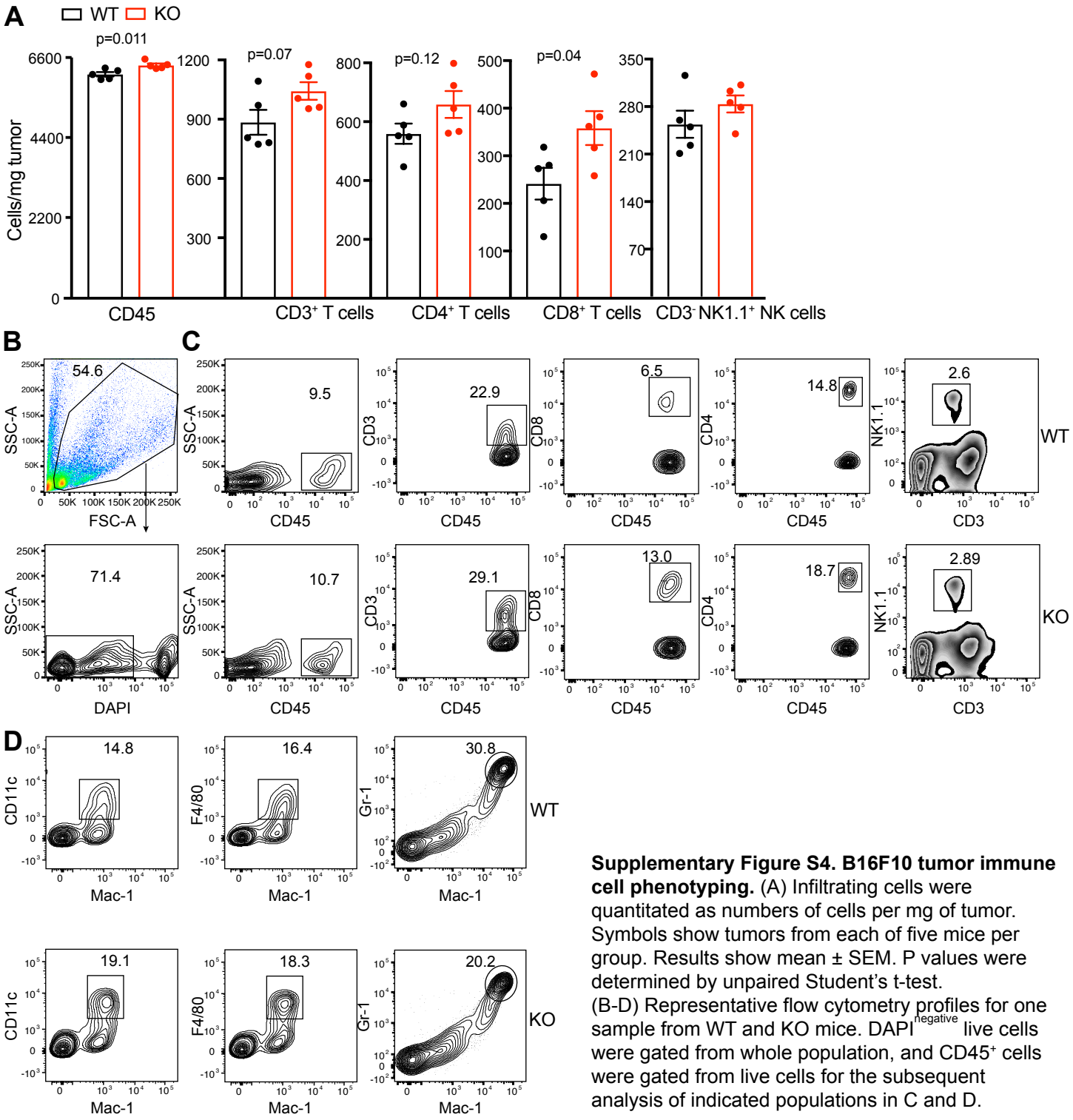

Supplementary Figure S4. B16F10 tumor immune cell phenotyping. (A) Infiltrating cells were quantitated as numbers of cells per mg of tumor. Symbols show tumors from each of five mice per group. Results show mean ± SEM. P values were determined by unpaired Student's t-test.
(B-D) Representative flow cytometry profiles for one sample from WT and KO mice. $DAPI^{negative}$ live cells were gated from whole population, and $CD45^+$ cells were gated from live cells for the subsequent analysis of indicated populations in C and D.

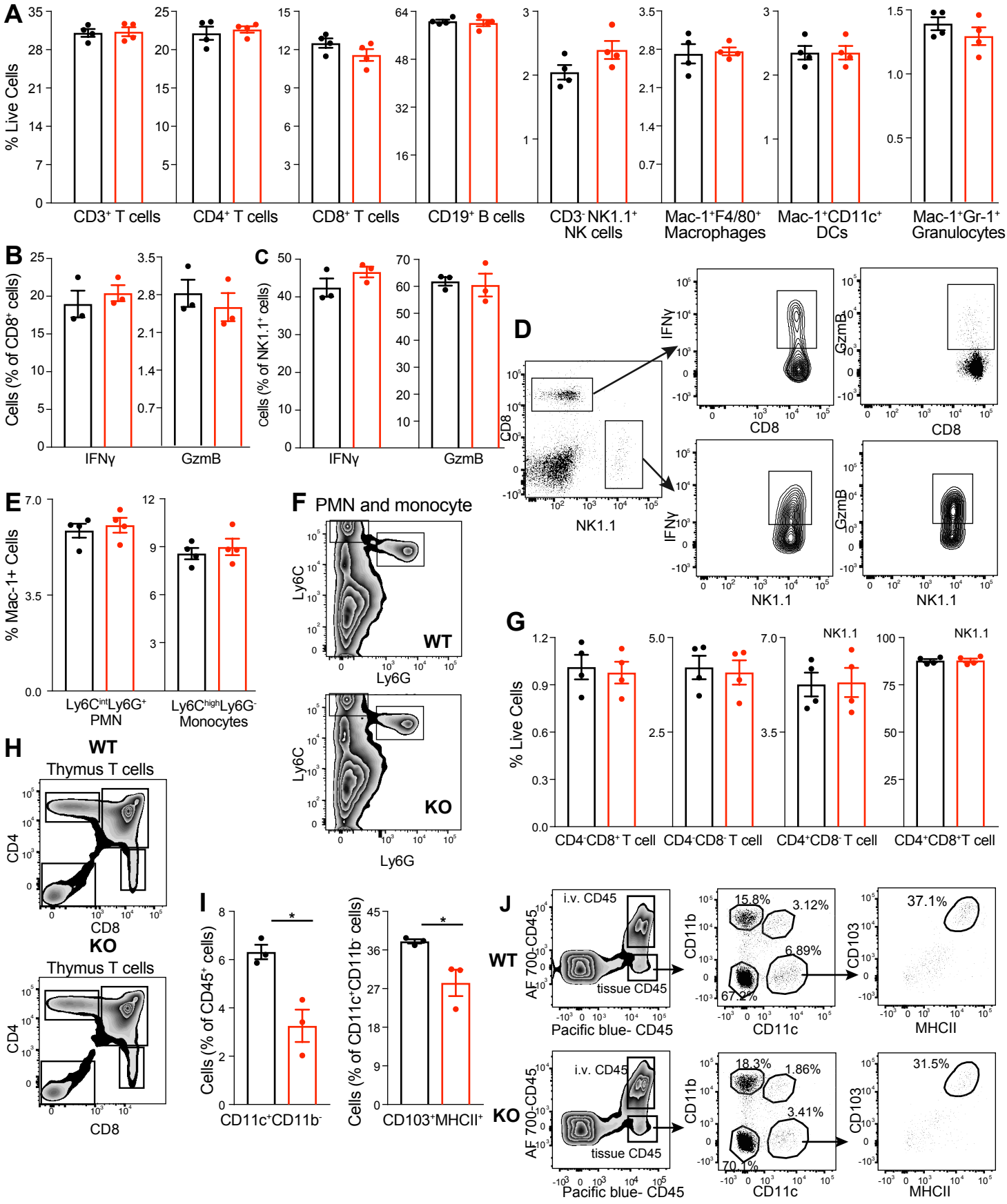

Supplementary Figure S5. Lrrc33$^{-/-}$ mice had equivalent compositions of major immune cell subsets in speen and thymus with WT mice, but not in lung. (A-H) Cells were isolated from spleen (A-F), thymus (G-H) or lung (I-J) of 7 week old mice. Each indicated cell type was quantitated as % of total live cells, % of Mac-1+ cells or other cell subsets. (I-J) Lung extravascular dendritic cell analysis. Cells were gated on live, intravascular AF 700-CD45$^-$/extravascular Pacific blue-CD45$^+$ (tissue resident cells), and downstream gates as indicated. Symbols show each of 3-4 mice per group. Results show mean ± SEM. P values were determined by unpaired Student's t-test. (D) shows representative gate strategy of activation markers of WT. CD8 and NK cells were gated out for IFNγ and GzmB analysis. KO had similar frequencies. (F, H, J) show representative flow cytometry profiles for one sample from WT and KO mice. Data represent two independent experiments. * p<0.05 as determined by unpaired Student's t-test.

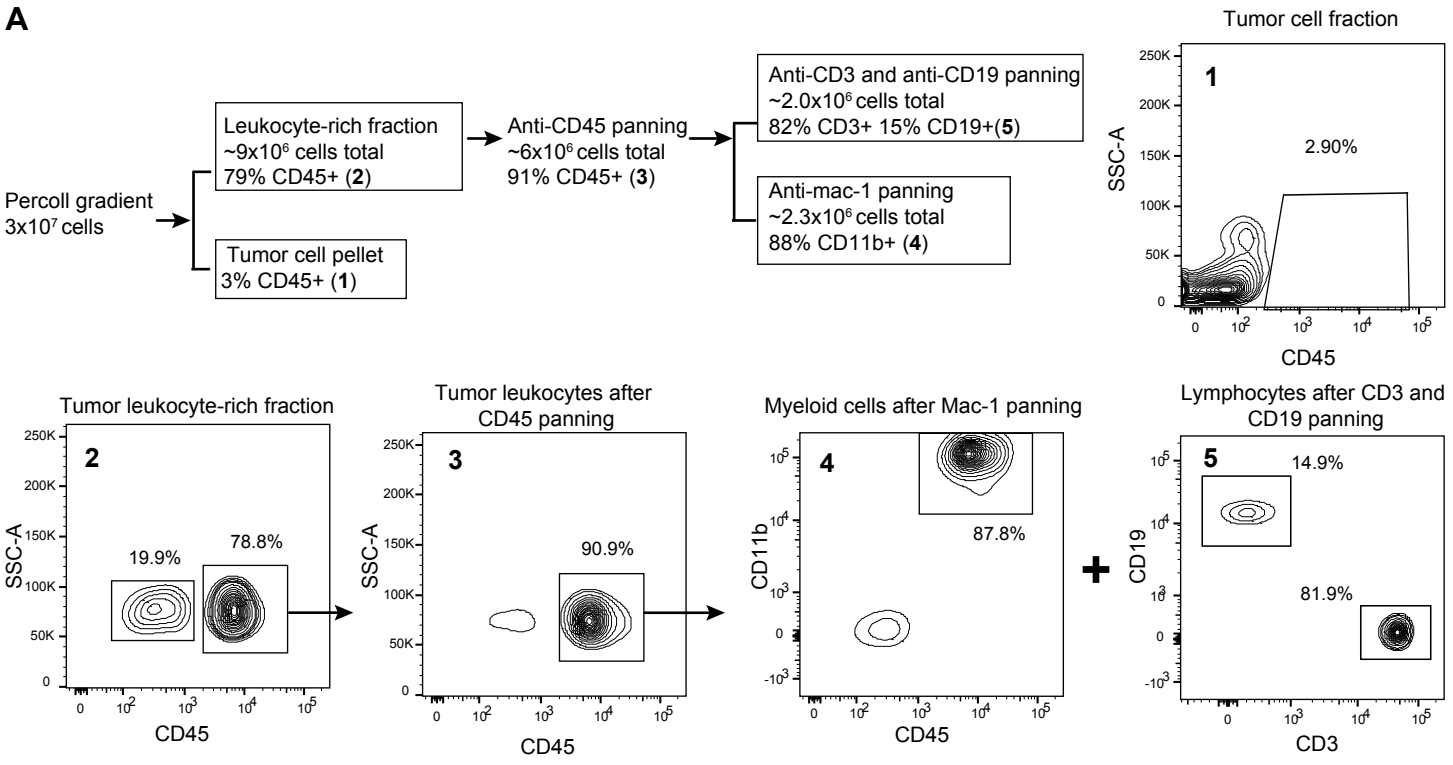

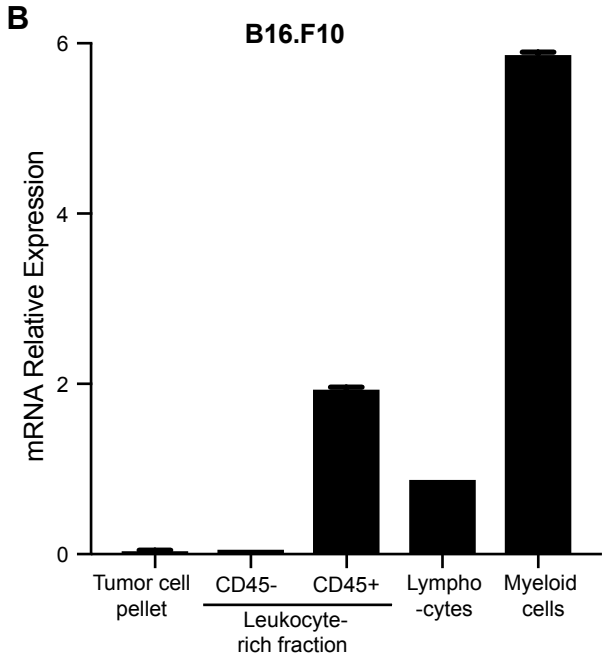

Supplementary Figure S6. Lrrc33 mRNA distribution analysis in B16F10 tumor. (A) Cells were isolated by centrifugation at 1600g for 30min on a gradient with layers of 40 and 70% percoll. The leukocyte fraction was taken at the interface between the 40% and 70% percoll layers and tumor cells were taken from the pellet and subsequently purified by panning. Purity was measured in panels **1-5** by flow cytometry. (B) Lrrc33 mRNA expression relative to GAPDH in the indicated cell types determined by RT-PCR as 2-ΔCt x 10000 (ΔCt = Ct gene of interest - Ct gapdh) and shown as mean ± difference from mean of duplicate samples.